THE DESIGN, CONSTRUCTION, AND VALIDATION OF NOVEL ROTATING WALL VESSEL BIOREACTORS

A Thesis
Submitted to
the Temple University Graduate Board

In Partial Fulfillment
of the Requirements for the Degree
MASTER OF SCIENCE IN BIOENGINEERING

---

by
Michael A. Phelan
Diploma Date May 2018

Examining Committee Members:

Peter I. Lelkes, Advisory Chair, Department of Bioengineering
Yah-el Har-el, Department of Bioengineering
Ruth Ochia, Department of Bioengineering

ABSTRACT

The rotating wall vessel (RWV) bioreactor is a well-established cell culture device for the simulation of microgravity for suspension cells and the generation of spheroids and organoids. The key to the success of these systems is the generation of a delicately maintained fluid dynamics system which induces a solid body rotation capable of suspending cells and other particles in a gentle, low-shear environment. Despite the unique capabilities of these systems, the inherently delicate nature of their fluid dynamics makes the RWV prone to multiple failure modes. One of the most frequently occurring, difficult to avoid, and deleterious modes of failure is the formation of bubbles. The appearance of even a small bubble in an RWV disrupts the crucial laminar flow shells present in the RWV, inducing a high-shear environment incapable of maintaining microgravity or producing true spheroids. The difficulty of eliminating bubbles from the RWV substantially increases the learning curve and subsequent barrier-to-entry for the use of this technology. The objective of this study is to create a novel RWV design capable of eliminating the bubble formation failure mode and to demonstrate the design's efficacy. The tested hypothesis is: "The addition of a channel capable of segregating bubbles from the fluid body of the RWV will protect its crucial fluid dynamics system while enabling the growth of consistently sized and properly formed cell spheroids, improving ease of use of the RWV and decreasing experimental failure."

This thesis is dedicated to my fiancée Kelsey Manahan. Her continuous support and enduring love made the effort behind this thesis not just possible but also worthwhile.

TABLE OF CONTENTS

Page

LIST OF TABLES

LIST OF FIGURES

Figure Page

CHAPTER 1

INTRODUCTION

The nature of life is fundamentally three-dimensional. From the conformational folding of proteins to the positioning and function of sub-cellular structures to the massive and incredibly sophisticated organization of cells and their matrices in eukaryotic tissues, life has evolved to utilize the entirety of the time-space it occupies. With a century of use and thousands upon thousands of ground-breaking discoveries, two-dimensional cell culture monolayers are the paradigm of biomedical tissue culture research [1]. Despite their entrenched position as the gold standard of *in vitro* research, their inherent "two-dimensionality" is rapidly becoming insufficient to study the increasingly intricate subtleties uncovered by our species' pursuit of the nature of our three-dimensional existence [2]. To extend humanity's capacity to replicate life in a scientifically controlled method, researchers have turned to the use of three-dimensional cell culture methodologies. In the process, they have unearthed revolutionary potential in tissue engineering, drug discovery, biological modeling, microbiology, genomics, stem cell and developmental biology, personalized medicine, and even direct *in vivo* therapeutics [3]–[5].

One of the most sophisticated tools in the culture of 3D tissues is the rotating wall vessel bioreactor or RWV [6]. Initially designed by NASA to culture cells in a simulated microgravity environment similar to that experienced in Earth-orbit and outer space, it is used today for both 3D tissue culture and the study of the effects of microgravity on cellular systems [7]. With science's expanding interest in 3D tissue study and humanity's thirst to colonize the stars thus far unquenched, the RWV represents an intersection of cutting edge technology that demands to be explored and expanded to the pinnacle of its potential.

1.1. Organoids and Spheroids for *in-vitro* and *in-vivo* Medical Research

The applications in the burgeoning field of 3D biological studies have multiplied from a diverse array of categories. One of the oldest types of 3D culture is tissue grown in a thick layer of extracellular matrix-like gels, scaffolds, or biomaterials [8]. The cells, either mixed in or seeded onto the scaffold, proliferate and migrate, surrounded by the material on all sides; their integrins and focal adhesion points adhering to the matrix in a way similar to their natural orientation. Alternatively, to produce structures more closely resembling live tissue, researchers abandon creating a new system and simple rely on nature to produce the scaffold for them. Decellularization is the process in which actual organs, extracted from recently deceased animals, are treated with a series of chemicals to remove cells and immunologically active peptides, ideally leaving only the extracellular matrix behind [9], [10]. These scaffolds can then be "recellularized" with cells derived from any source or patient. The chief application of the decellularization/recellularization approach is the implantation of tissues and organs into the patient providing the cells to produce a perfectly immunologically compatible donor tissue [11]. The final kind of 3D culture to be discussed, and one of particular significance in this thesis, is a large aggregation of cells referred to as either organoids or cell spheroids. To describe the importance of spheroids and organoids, we will first define and classify their types, then describe their current applications and future potential, and finally discuss their mechanisms of formation and subsequent methods of generation.

First, it is critical to define the cell spheroid and the organoid. Both the cell spheroid and the organoid are, in the broadest possible terms, large, self-assembling structures of hundreds to thousands of aggregated cells in a near spherical shape in the absence of

external adhesion or shear forces [12]. The self-assembling nature of these aggregates imparts unique properties by ensuring the activation of cell-cell interactions and membrane attachment proteins that are present in every biological tissue. Although the terms are sometimes used interchangeably, traditional definitions distinguish the two types in that cell spheroids are formed from simple cultures of fully differentiated cells while organoids are much more complicated and can be produced with actively differentiating stem cells. Ultimately, organoids will much more closely resemble the biochemical and cellular environments of a true, whole-organ tissue with multiple organized cell types derived from the same stem cells [13]. These differences mean cell spheroids are usually substantially easier to prepare but have fewer and narrower applications than organoids. Due to these differences, the applications of spheroids and organoids will be discussed separately.

With their ease of production and simple characteristics, the cell spheroid is the most direct advancement and one of the 3D systems most similar to traditional 2D cultures. From the perspective of being effective monocultures similar to traditional tissue cultures, two broad sub-categories of spheroids can be described: spheroids produced of healthy cells which resemble direct interactions between a handful of cells; and tumor or cancer spheroids which, even as macroscopic structures, still resemble the pathophysiological nature of large non-vascularized tumors *in vivo* [14]. Although these two subcategories possess similar applications, it is necessary to discuss the two separately due to key limitations in their crossover.

Tumor spheroids, in current literature, appear to have a more restricted set of applications, but tend to more closely resemble actual *in vivo* outcomes. Unsurprisingly, due to the tendency for tumors to be unwanted guests in their hosts, drug screening and

cancer treatment testing are key applications of tumor spheroids with several unique advantages over traditional systems. Due to the lower surface area-to-mass ratio of natural 3D tissue compared to a 2D system, spheroids are ideal for the validation of cancer drug delivery [15]. Because cell targeting drugs need to pass through every cell's membrane, the concentration of drugs in a cell is typically lower than in the extracellular fluid. In a 3D system, drug availability to cells in the interior of the spheroid or tumor is always lower than to the more exterior cells. Subsequently, a diffusive gradient is formed. The ability for a chemotherapeutic to maintain its efficacy through the lowest concentration it will likely encounter in any cell is critical to its capacity to fight a tumor. Indeed, exposure of a cancer cell to low concentrations of a chemotherapy chemical can promote "evolutionary resistance" to the drug, effectively making the patient's cancer more virulent [16].

The limited exposure of cell mass relative to surface area is relevant to several other unique characteristics of cell spheroids. Not only do drugs and pharmaceuticals diffuse though the spheroid in a gradient, but so do nutrients like oxygen and glucose [17]. Figure 1 shows an example of how these gradients form. Sufficiently sized spheroids effectively have three distinct regions, a normoxic, hypoxic, and necrotic zone depending on the distance of the cells from the surface and the amount of time the cells have been exposed to low oxygen conditions. The hypoxic and necrotic regions appear in actual tumors, and thus, are critical to understanding the behavior of tumors *in vivo*. The appearance of these low oxygen regions leads to increased DNA damage, change in proliferation and migration rates, and a host of expression changes [18]. The sum of the changes that occur in cancer cells due to hypoxia is dramatic. Due to a massive cascade mediated by Hypoxia Inducible Factor, a cancer cell starved of oxygen may undergo a mesenchymal-epithelial transition,

likely the root cause of tumor metastasis [19]. Understanding cancer in its native three-dimensional context is crucial to overcoming its most dangerous aspects.

Finally, *in vitro* testing of tumor spheroids enables a true approach to personalized cancer medicine. Because the tumor cells to be cultured can be sourced from anywhere and because their final 3D structure so closely replicates a cancer's natural arrangement and composition, cells biopsied from a patient can be grown into independent tumor spheroid colonies [20]. Since the pathological genetics of every patient's cancer is so unique, performing pharmacological tests on those cells may be the only way to truly predict their response to particular treatments. Perhaps, one day, a cancer biopsy can be taken, cultured into spheroids, and tested in real time to determine the best course of action for treating each individual patient.

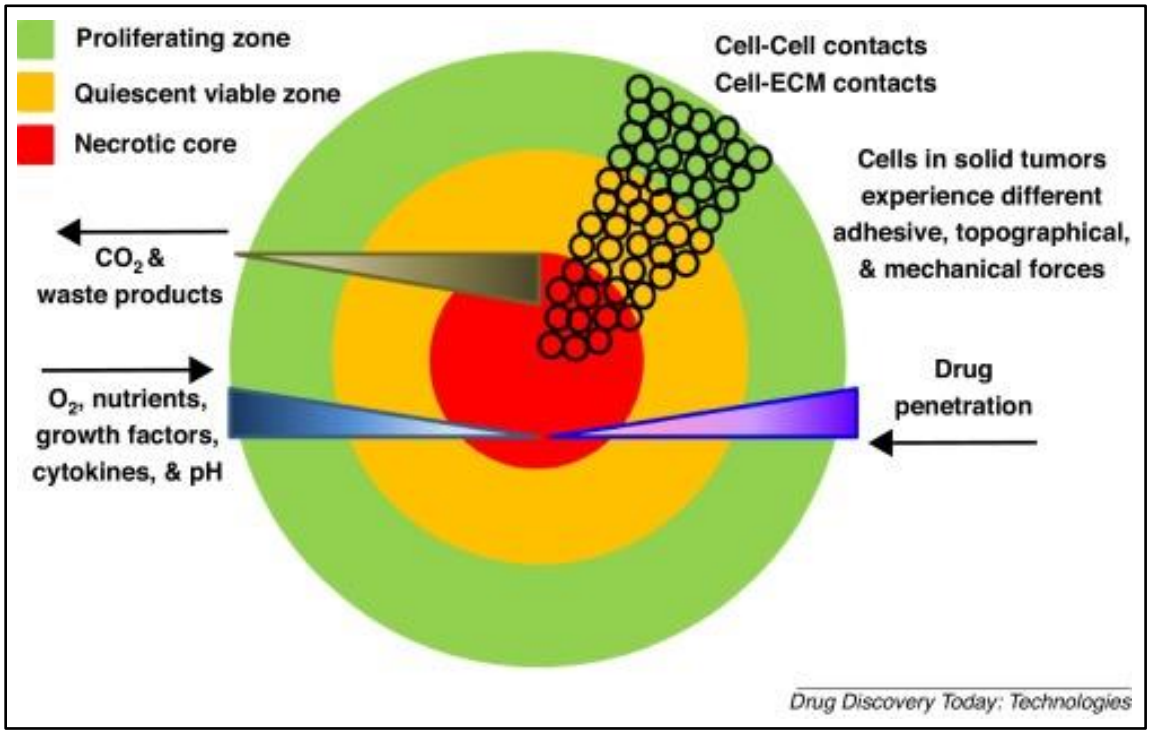

Figure 1: Diffusive gradients in cell spheroids. [17]

Outside of the limited scope of cell spheroids for cancer modeling, a broader range of applications for healthy-cell spheroids exist. Of the many dozens being investigated, one of the most promising applications is the implantation of autologously derived spheroids for clinical regenerative medicine [21]. The general concept of spheroid implantation follows the standard regenerative medicine model of: remove cells from a patient, culture the cells *in vitro* and induce desired changes, and re-implant the cultured cells back into the patient. However, when spheroids, supported by a variety of bioactive gels and materials, are implanted, their propensity to remain in the target tissue, their release of therapeutically relevant signaling cascade activating molecules, and their ability to diffuse into target tissues make them vastly superior to the implantation of single cell suspensions [22], [23]. Spheroids, made of mesenchymal stem cells or healthy mature organ cells, when implanted into a diseased tissue, are intended to activate the body's natural regenerative response and enable a sick or even potentially failing organ to return to healthy function. Early *in vivo* testing of this technology on animals has shown promising results and may open the door to advanced, personalized treatments of organ failure in years to come [24].

Despite the vast potential for the medical application of the spheroids, their complexity and long-term capacity for discovery pale in comparison to those of the organoid. As stated above, the organoid starts as an aggregation of actively differentiating stem cells cultured according to much more difficult and expensive procedures than those for simple spheroids. When treated with precise morphogens and growth factors, these stem cells can be pushed to organ-specific fates. These fates might include differentiation into multiple mature cell types, with their final placement in a 3D environment remarkably similar to the structure of the living body [25]. Figure 2 shows the arrangement of cells

differentiated from induced pluripotent stem cells in an organoid to produce an artificial retina [26]. The green stain, for rhodopsin, describes the location and organization of photoreceptor cells, while the red stain, for glutamine synthetase, stains for Müller glia cells. The arrangement and layering of these cells is not only remarkably similar to the arrangement of a true retina, but even the direction of the facing of the tissue mimics the orientation of cells in the optic cup during embryonic development.

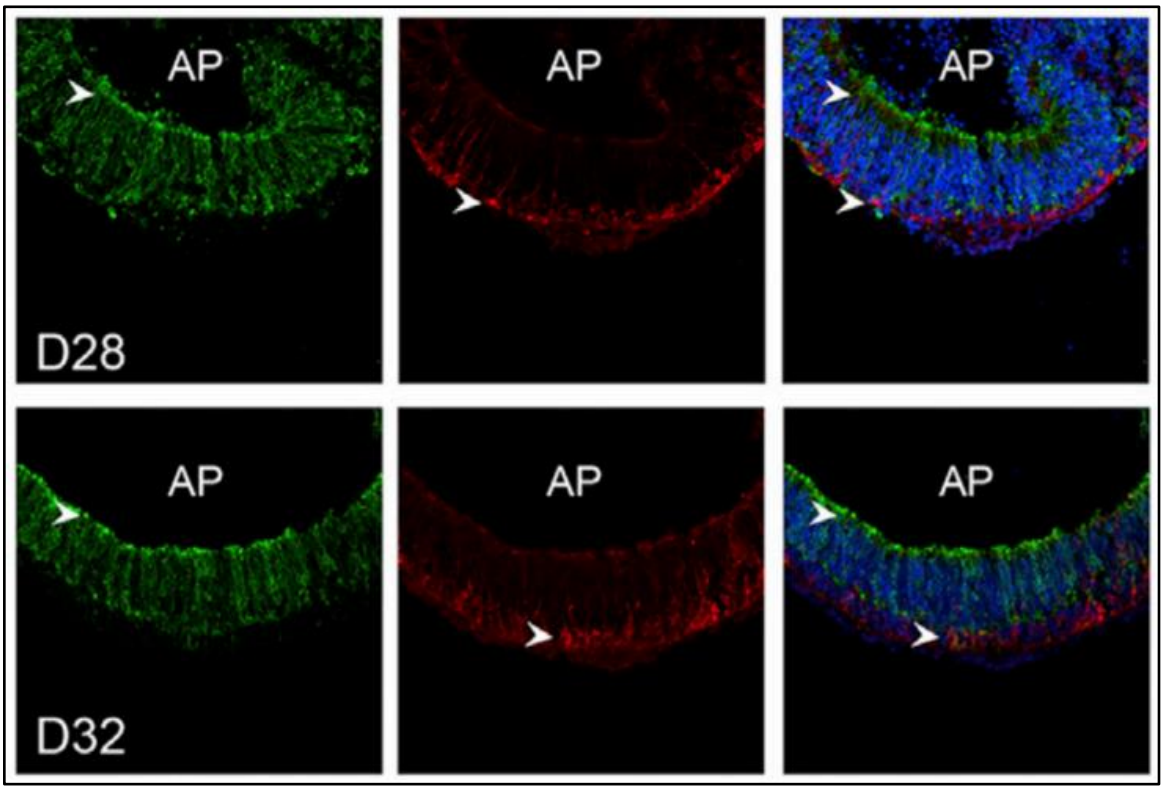

Figure 2: Green = Rhodopsin, Red = glutamine synthetase, Blue = DAPI – The arrangement of cells in this organoid closely resembles in vivo tissue. 28 and 32 days of cell culture respectively.

This capacity to produce tissue-like constructs offers multiple incredible applications. Virtually all of the applications listed above effectively be accomplished by organoids as well as, or in some cases better than, cell spheroids. Additionally *in vitro*

approaches to whole tissue and multicellular drug responses to dozens of tissue types, responses to toxins during embryogenesis, and personalized medicine approaches to rare genetic diseases (to name a few) offer unparalleled levels of sophistication and complexity relative to virtually any other *in vitro* technology in common research literature today [27], [28].

1.2. Microgravity and the Cellular Response

While Earth-based biomedical research tends to dominate the minds and markets of modern biology, humanity's increasingly realistic visions of permanent extraterrestrial settlements indicate that the gaze of today's life scientists may soon have to adjust from the microscope to the telescope. The idea of human life in space is truly tantalizing, but, as with any major advancement, is rife with unexpected and seemingly insurmountable obstacles, particularly the pathophysiological response of the human body to long-term spaceflight. Amongst the sources of these space-based health hazards are hypoxia, acceleration forces, high radiation, and weightlessness [29]. While high radiation found outside of the safety of Earth's magnetic field is an easily understandable and long expected source of health concerns, the damage associated with weightlessness, also referred to as microgravity, was quite unexpected to early astro- and cosmonauts and is potentially even more detrimental.

In the 3.5 billion years of evolution on the surface of the Earth, the environment has changed immensely. The shifting of tectonic plates, wildly fluctuating temperatures, the appearance of high concentrations of oxygen in the atmosphere, and the rise of flora and fauna have, at least on geological timescales, necessitated constant adaptation. In spite

of the propensity for life to adapt to its changing landscape, one true, persistent condition since our primordial environment has been the presence of a constant acceleration towards the core of our planet at about 10 meters per squared second. To separate ourselves from the biological imperative of gravity between the biochemical and organ system scales may require a change in the course of biological evolution unseen since the rise of the hominids. To circumvent the hundreds or thousands of generations needed to make this change occur naturally, governments and private organizations will need to engage in a concerted, massive, and highly organized effort to improve our understanding of the biological response to microgravity and to produce medicines and techniques to counteract it.

Microgravity is defined as an ultra-low gravity environment encountered through gravitation nullification, like through freefall, or through extreme distance from a sufficiently massive object to reduce its gravitational effect [30]. Six orders of magnitude greater in force is 1 gravity, the level experienced on Earth. For any animal on our planet, the effects of gravity help to regulate systems from sub-cellular levels through the structure of the entire body. Although modern astronauts engage in constant, rigorous exercise to combat these effects, this behavior provides minor and incomplete treatment. The systems known to be detrimentally affected by low-gravity exposure (and thus must be regulated by 1 G on Earth) include, but are not limited to, the heart, the immune system, the skeletal system, the brain, the eye, the kidney, cell division, stem cell differentiation, wound healing, the reproductive system, and embryonic development [31]–[34]. Clearly, the scope and variety of these issues indicate complex and multi-level interactions that must be heavily studied before serious headway can be made. Of the array of negatively impacted systems listed above, the scope of this introduction will be to describe the precise

mechanisms and degrees of severity for two key processes that are disrupted, the skeletal system and embryonic development.

The skeletal system is much more than a simple frame to support the rest of our body's functions. Not only do the bones facilitate movement and protection, they also serve as endocrine regulators, production sites for red blood cells, storage locations for minerals and lipids, and a host of other roles [35]. The mineral structure of the bone is supported by osteocytes, fully matured bone deposition cells, but the overall structure is constantly remodeled by a tightly controlled and choreographed push-pull of deposition and resorption by osteoblasts and osteoclasts, respectively. Although there are multiple sources of regulation of bone remodeling, one of the primary sources of both repair and regeneration is mechanical stimulation [36]. The translation of this mechanical stimulus into a biochemical output that produces biological change is referred to as mechanotransduction. The mechanotransduction leading to the regulation of bone remodeling is partially mediated by integrins, concentrated into focal adhesion points, that produce downstream cytoskeletal and eventual genetic expression changes through the ERK 1/2 pathway. This sensory feedback system enables the bones to sense when "weak" points that need to be repaired appear in the matrix and when changes in environment or behavior demand greater bone deposition for increased or decreased activity. Like so many things in life, the skeletal system is closely monitored and that ensures no greater amount of energy or nutrients is spent than is absolutely necessary.

In microgravity, this elegant system for bone homeostasis becomes a serious liability. With no impacts against the bones due to walking, running, lifting heavy objects, or even sustaining the weight of one's own head while standing up, the demand for

deposition of bone mineral drops to practically nothing, while bone resorption increases dramatically [37]. Several studies have indicated that in microgravity, an astronaut can be expected to lose between 0.5% and 5% of their total bone mass each month [38]. In fact, over the course of a long-duration spaceflight, three astronauts lost 30% of their bone mass each. With the importance of the skeleton for health, the significant damage done to it in microgravity should be a serious concern to anyone who has ever dreamed of going to space. While the bone is one example, this loss of mechanotransductive force negatively impacts any organ system that is capable of sensing it, from the heart to the immune system [39], [40].

Though the idea of one's own bones melting away due to lack of stimulation is a concerning enough thought, microgravity's potential for disrupting embryonic development changes the feasibility of a self-sustaining extra-terrestrial colony from simply unhealthy to practically impossible. The disturbance of embryonic development is due, partially, to improper stem cell differentiation in microgravity [41]. Conceptually, it is of no surprise that mechanotransductive forces can determine the fate of a stem cell. When free migrating mesenchymal stem cells need to undergo differentiation, the stiffness of the tissue they encounter is key to determining their final fate [42]. With multiple final fates that are established under tightly regulated and time-sensitive developmental conditions, pluripotent embryonic stem cells require precise mechanotransductive feedback in conjunction with specific growth factor gradients to produce the correct mature tissues [43]. Additionally, microgravity does not simply interfere with cell-ECM interactions. Because the organelles and sub-cellular structures of the cell are situated amongst a net of cytoskeletal components, their orientation and motion inside of the cell

can itself produce its own internal mechanosensitive effect [44]. This effect will lead to substantial genomic, proteomic, and metabolic changes inside of a single cell, grossly affecting pluripotent differentiation.

The effect of microgravity on reproduction and embryonic development has been well described in literature. In 2011, Wu, et al. described how simulated microgravity led to a disruption of spindle organization of oocytes, interrupting meiosis and decreasing oocyte maturation more than eight-fold versus control [45]. As a result, before an embryo is even fertilized, lower gravity will invariably reduce fertility. Assuming embryonic development can begin, things do not improve. A 2009 Wang, et al. paper describes how exposure to microgravity can substantially increase lethality of early-stage mouse embryos by elevating levels of phosphorylated SAPK/JNK, a protein associated with cell stress [46]. This effect can lead to a two-fold decrease in total embryo cell count and a four-fold increase in cell apoptosis, substantially reducing embryo viability and likely producing long-term developmental defects. Several such defects (amongst dozens of others) have been described, including potential dedifferentiation of cardiac progenitor cells, decreased maturation of oligodendrocytes, and substantial interference with natural angiogenesis [47]–[49]. It cannot be stressed enough that unless the biological constraints of space exploration are resolved, no degree of technological advancement in aerospace or rocket engineering will make long-term space colonization feasible.

1.3. RWV Bioreactor Function and Use

Earth-based organoid and spheroid research and space-relevant microgravity studies are linked by a common, incredible technology, the rotating wall vessel bioreactor.

The rotating wall vessel bioreactor, or RWV, is a device that was first developed by NASA in the 1980s as a method to simulate microgravity conditions experienced by cells being transported back from true microgravity conditions in orbit [50]. Soon, it was demonstrated that the RWV had the capacity to simulate the cellular response to microgravity without ever leaving the ground. It was also observed that the suspension of cells in a low-stress environment allowed for the formation of groups of cells adhering to one another as 3D aggregates. The need to further develop and market this promising technology led to the formation of Synthecon, Inc., a private company offshoot that specializes in the manufacture and sale of RWV bioreactors and similar 3D cell culture devices.

The RWV consists of several key components. First, there is a central, watertight, cylinder-shaped cavity which holds cells suspended in a volume of nutrient-containing media. Next, there is either a gas permeable membrane or gas infusion column capable of oxygenating the cells and maintaining correct CO2 levels. Next, there are several filling and emptying ports affixed to the front of the bioreactor. Finally, the bioreactor is attached to a motorized drive system capable of rotating the bioreactor around the central axis of its cylinder at a low and constant speed. Figure 3 shows the design of several Synthecon bioreactors of different lengths and volumes along with a motor drive (called a RCCS-4) capable of running four bioreactors simultaneously [51].

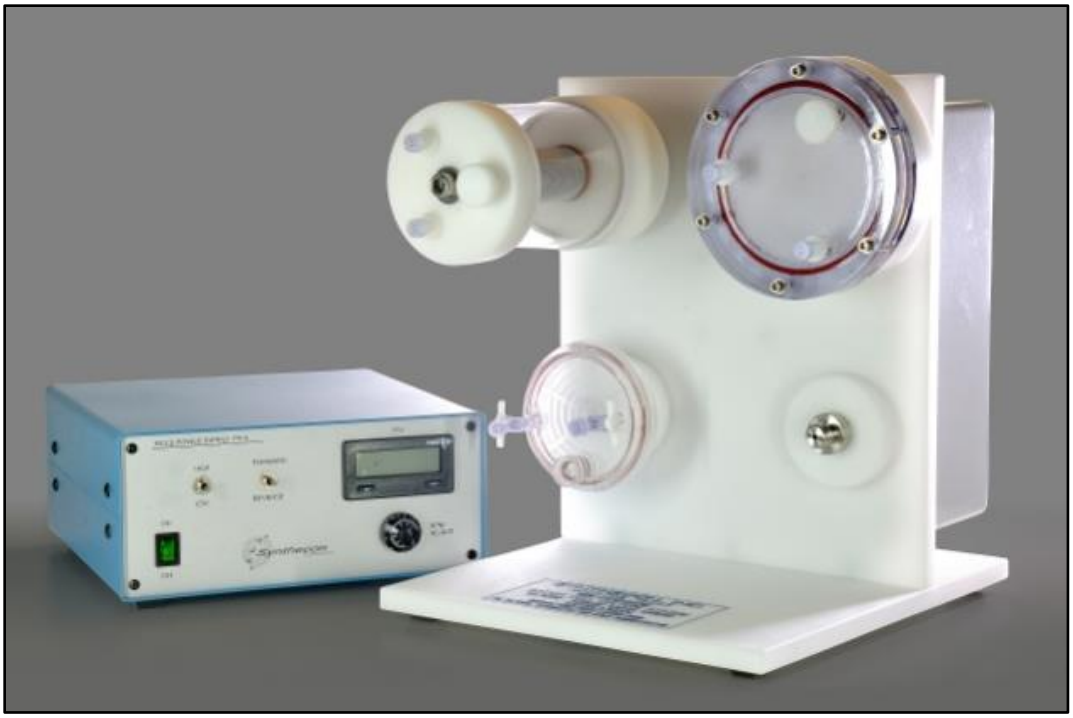

Figure 3: Several RWV bioreactors with motor drive. [51]

The RWV relies on the establishment of a delicate fluid rotation that suspends cells and aggregates with it as it rotates. This rotation induces a clinostat effect, where objects in constant circular rotation perpendicular to the ground will eventually have their experienced rotational vector averaged to near zero, literally microgravity [52]. With its capacity to simulate microgravity and generate spheroids and organoids, the RWV has found a niche in a multitude of biomedical and space biology research applications.

1.3.1. RWV Mechanics

The process by which a simple rotating tube is capable of simulating the environment more than 400 kilometers above the Earth's surface can be rather abstract. It must be considered first with respect to its fluid dynamics and then with respect to the behavior of individual objects or particles the fluid dynamics interacts with. The fluid

motion is established slowly over time. First, as the walls of the device begin to move, inertia dictates the fluid it contains will stay at rest, as if no rotation took place whatsoever [53]. Due to the no-slip condition, the tendency for the smallest divisible layer of a fluid to have zero velocity relative to the solid surface boundary, the outermost of a series of concentric layers of fluid, begins to move in time with the walls. This shell only truly forms if a fluid-solid boundary exists against the entire interior perimeter of the vessel. As the outermost fluid shell rotates with the wall, it drags the next outermost shell of water with it. As shown in Figure 4, over time each consecutive shell begins to rotate in time until the entire fluid body is rotating as if the entire system was made of a single solid piece. This so called solid body rotation is a delicate fluid dynamics system, and while slow to form in its entirety, is key to the low-shear, microgravity environment so unique to the rotating wall vessel [54].

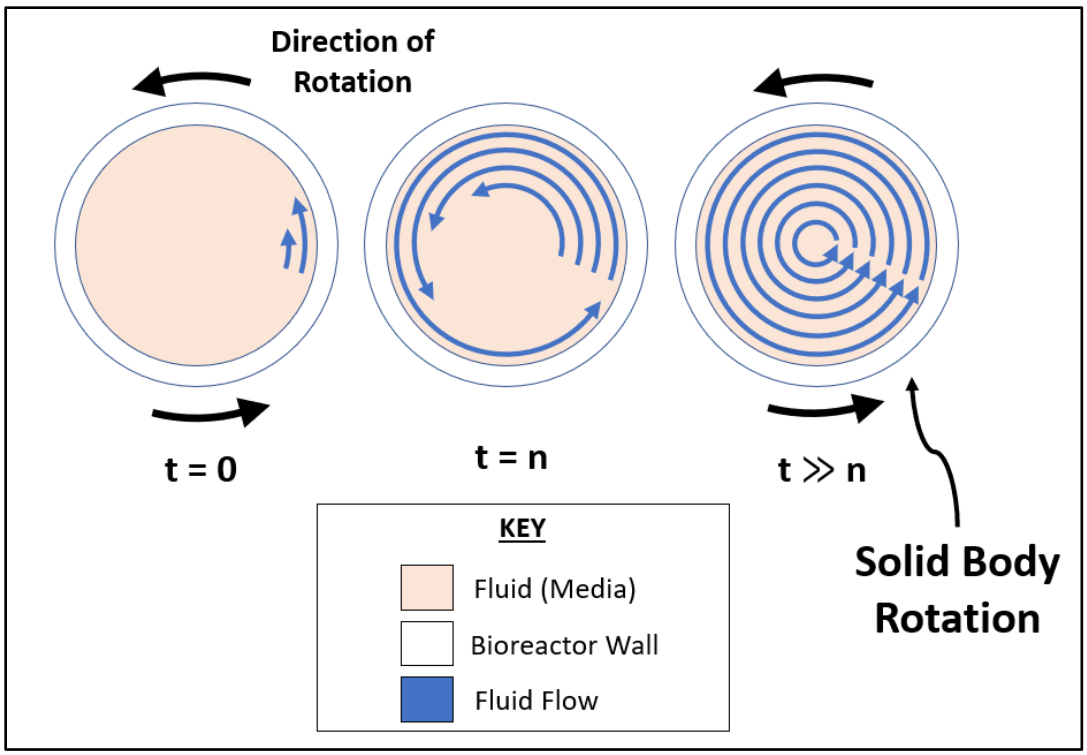

Figure 4: Generation of solid body rotation in an RWV.

The motion of a particle in a bioreactor that has just begun rotating does not follow the clean, concentric buildup of solid body rotation. Instead, the particle follows a wide, meandering, spiral trajectory until the fluid system reaches equilibrium. Figure 5, taken from a 2001 review, shows that trajectory path with a fixed frame of reference (C), i.e. with the camera affixed to the bioreactor, and a rotating frame of reference (D), i.e. the camera stationary relative to the ground [55]. Of note, (C) shows that after an extended period of time, the expected trajectory of the particle is effectively static versus a fixed position of the bioreactor. This eventual stasis means that the particle moves in an even circle around the central axis of the bioreactor at the same rotations per minute that the system is moving. With a perfectly circular path the sum of the gravitational vectors approaches zero. With no velocity of the particle relative to the fluid, effectively no fluid shear occurs at the

surface of any particle. Thus, the low-shear, microgravity environment is established. While this environment is already ideal for organoid and spheroid generation, imperceptibly small amounts of mixing and rotation of media around the aggregates provides optimal nutrient availability, enabling the RWV to produce better and healthier organoids and spheroids faster and more consistently than any current aggregate generating technology [26], [56], [57].

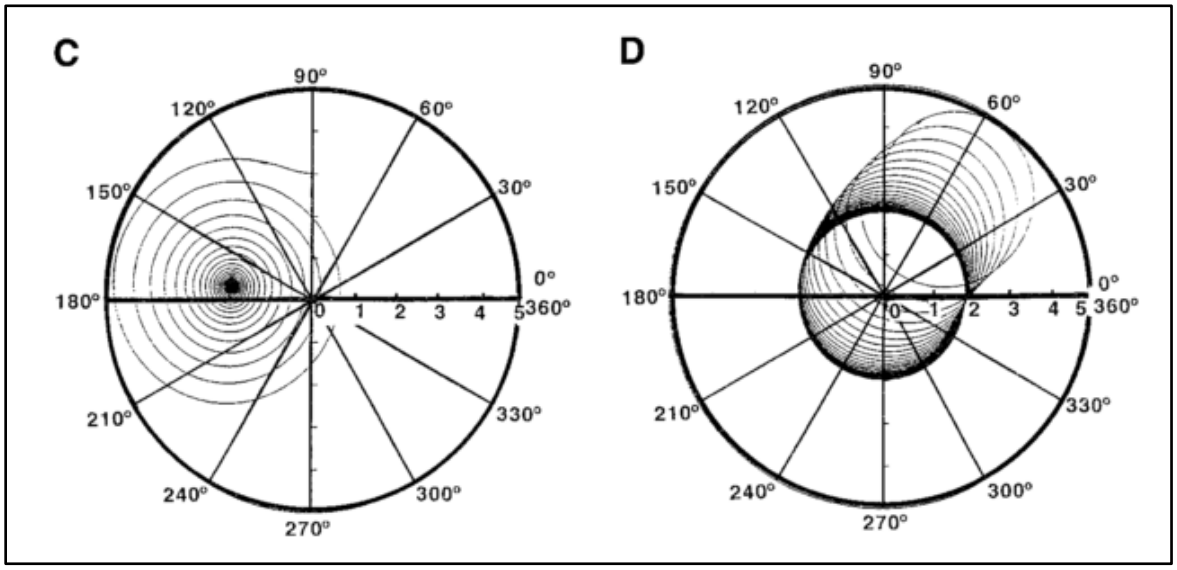

Figure 5: Projected trajectory of particle in an RWV over time in a fixed frame of reference (C) and in a moving frame of reference (D). [55]

1.3.2. Disrupted Fluid Dynamics and Turbulence

In order for the solid body rotation to exist, the no-slip interface between the wall and the fluid boundary must be complete around the inner perimeter of the wall. Should an airgap, referred to as headspace, exist at the top of the system, the laminar shells needed for solid body rotation do not form, and the predictable concentric, circular velocity vectors are replaced with chaotic turbulence. As the fluid attempts to rush around the air, its

velocity increases, a negative pressure develops behind the air opposite the direction of flow, and the system begins to mix and churn. Any hope for a circular rotation trajectory is obliterated, along with microgravity stimulation, and the rapidly changing fluid velocities through the system guarantee shear orders of magnitude higher than anticipated in an ideal system.

As described above, all RWV bioreactors have filling ports and a gas diffusion system. As such, through the filling and running of the systems, incredible care has to be taken to prevent the formation of an airgap system. Air can enter the system through improper clearing during preparation, the "holding" of a small pocket of air in one of the filling ports, or due to fluid leakage. Worst of all, because these systems are inherently and necessarily gas permeable, should the relative humidity of the incubator in which these systems run dip below 100%, even for a small period of time, diffusion of water vapor away from the system will create negative pressure in the bioreactor that will rapidly be replaced by ambient air leaving behind a small bubble. For decades, researchers employing the RWV have discussed the importance of and dexterity required in the removal of air bubbles from these bioreactors [31], [55], [58]–[63]. Despite this history, no detailed description of the significance of turbulence due to bubbles has been found in an in-depth literature search and no simple yet effective modifications have been made to eliminate them.

1.3.3. The HARV

One of the lowest cost and easiest to use RWVs produced by Synthecon, Inc. is the disposable HARV or High Aspect Ratio Vessel. Aspect ratio is the ratio of the width to the height of an object. In the case of the HARV, this high aspect ratio dictates that the diameter

of the cylinder is substantially higher than its height, somewhere in the range of 10:1. While the standard RWV relies on a pump to drive the perfusion of gas through the media, the application of a gas permeable membrane against the entire back of the HARV enables it to passively diffuse gases through the short distance between the front and back bases of the cylinder. Being the simplest form of the RWV, the HARV will be the focus of this thesis' attempt to design and produce a form of the RWV that is less detrimentally affected by bubbles, in hopes of promoting research and improving results of scientists and engineers investigating cell aggregates for medicine and microgravity for space exploration.

CHAPTER 2

AIMS OF THE RESEARCH

This thesis seeks to design and implement solutions to correct the problem of bubble formation in these systems while simultaneously introducing several ancillary advantages such as increased ease of use and positive identification of experimental failure. The new designs will be accompanied with mathematical modeling to ensure that the sensitive microgravity dynamics are not disrupted. Next, the novel designs will be fabricated into practical devices with demonstrated capacity for successful cell culture. Finally, simulated and actual cell culture will validate the above advantages of the novel bioreactor designs versus existing technology and confirm their ability to maintain the unique low-shear, continual free-fall microgravity analog environment that defines RWV bioreactors. This will all be accomplished within the framework of the hypothesis: "The addition of a channel capable of segregating bubbles from the fluid body of the RWV will protect its crucial fluid dynamics system while enabling the growth of consistently sized and properly formed cell spheroids, improving ease of use and decreasing experimental failure."

2.1. Specific Aims

Aim 1: Model, design, and fabricate traditional and novel rotating wall vessel (RWV) bioreactors.

2.1.1. Outline the key design criteria and characteristics required for the fabrication of an RWV bioreactor and describe the requirements of a bubble removal system.

2.1.2. Design the fabrication of traditional and novel bioreactors.

2.1.3. Describe the behavior of fluid flow in both design types using mathematical modeling and computational fluid dynamics.

2.1.4. Fabricate the bioreactors and write handling protocols required for their use.

Aim 2: Validate the capacity for novel bioreactors to meet or exceed the performance of existing RWV systems in multiple cell culture parameters.

2.1.5. Use visible, colored alginate beads to confirm modeled fluid behavior in both types of bioreactors and to observe for any unexpected behavior.

2.1.6. Demonstrate that the materials used in the construction of these vessels do not induce a cytotoxic response in cell culture.

2.1.7. Confirm the capacity of the novel designs to produce cellular spheroids and to compare them to traditional designs.

2.1.8. Intentionally induce the common bubble failure mode for traditional RWV bioreactors and compare to the novel designs.

2.1.9. Describe new failure modes that may occur in the novel designs, such as loss of cells from the system, and perform cell culture experiments to determine their probability and severity.

2.2. Rationale

The intent of the above Aims and sub-Aims is to build a superior RWV bioreactor in experimental robustness and experience-based barrier to entry by systematically following an engineering design process. The problem is stated, a solution is designed, the

design is scrutinized and then built into a functional prototype, and the prototype is evaluated against a host of measurable parameters. Additionally, the novel bioreactor is built in conjunction with a traditional-style model using identical materials and techniques so direct comparisons can be assessed.

CHAPTER 3

MATERIALS AND METHODS

3.1. Aim 1

3.1.1. Mathematical Modeling and Computational Fluid Dynamics

In order to determine the severity of the effects bubbles create in the rotating bioreactor and to describe the theory behind potential improvements to the bioreactor design, several simple mathematical models have been produced. These models do not take into account all physical effects but provide a description of the motion of particles and fluids under ideal conditions. These models describe the motion of a particle in a rotating bioreactor when disrupted by an air bubble, the motion of an air bubble in a linear tube that may act as a segregation device, the description of a state diagram of a bubble trapping modification, and the flow of media around an entrance to said bubble trapping modification. The employed mathematical models do not attempt to define new equations but exist as interpretations of rotational moment of inertia, sedimentation and buoyancy equations, the Hagen-Poiseuille pressure of a moving fluid equation, and the fluid shear viscosity formula.

Computational Fluid Dynamic (CFD) software was then employed to simulate expected fluid flow in the devices. CFD programs such as Fluent and CFX, packaged in ANSYS software, are widely used tools to estimate the motion of fluids and their interactions with solids, various types of motion, or other fluids. The CFD simulations were performed in Fluent, limited to a two-dimensional analysis, and attempted to accomplish four objectives. First, the fluid dynamics of a standard RWV bioreactor under perfect conditions was estimated in an attempt to establish a “baseline”. Second, the fluid dynamics

of a novel bubble removing design was simulated with no bubbles present to demonstrate if a novel design is capable of maintaining the expected fluid behavior under ideal conditions. Third, a bubble was introduced to the standard bioreactor to demonstrate the severity of its effects on the system. Finally, a bubble was introduced to the novel designs to determine if the system could function within its expected parameters. All CFD simulations used water as the fluid, were run under normal gravity, rotated at 10 rpm (~1 rad/sec), and were simulated for a minimum of 15 minutes to allow a fluid equilibrium to be established. It is worth noting that the simulated interactions between fluid and air in a fast-moving system are notoriously difficult. Subsequently, the third and fourth objective of this section may not provide a realistic representation of the system behaviors. Animations were exported using colored vector lines to represent fluid velocity.

3.1.2. Bioreactor Design

Once mathematical models conceptually demonstrated the feasibility of the novel bioreactor improvement capable of segregating bubbles, a design phase outlined the translation of the mathematics into a tangible device. The design phase had four key phases. First, a broad conceptualization of fabrication methodology was described to outline the scope and requirements of the design proper. Second, key dimensions such as volume and size were planned. Third, 3D CAD renderings were produced for the visualization of a completed device. Finally, engineering drawings were produced that were compatible with the laser cutting fabrication of both a standard bioreactor design and an improved bioreactor.

The novel portion of the new bioreactor is described as a simple channel that runs around the majority of the perimeter, like a concentric arc, in a clockwise manner. For

future reference, this is described as the “bubble catch channel”. The channel has an entrance opposite the location of the main emptying port of a standard HARV bioreactor. As the bioreactor rotates counterclockwise, any bubble that rises to the top of the system will enter the channel within one rotation and “float” to the back of the channel. Because the angle between the entrance to the channel and its back wall is well in excess of 180 degrees, the bubble’s buoyancy will never allow it to re-approach the bubble entrance. As such, any bubbles that enter the bubble catch channel will never be able to re-enter the main volume of the system and are unable to interrupt solid body rotation.

3.1.3. Bioreactor Construction

Once potential fluid systems had been described and their design completed, fabrication of finished bioreactors began. Both the standard and novel bioreactors were built primarily with 3/16” cell cast acrylic, which was cut using a Universal Laser Systems VLS 6.60 laser cutter. A front plate, back plate, and central ring were cut for each as well as a nut holder for the back, to be explained below. Pre-cut holes in the front bioreactor plates were tapped for screws using a quarter-inch tap. All acrylic was then annealed to increase tensile strength and resistance to cracking. To anneal, all acrylic was placed on parchment paper in a laboratory oven and brought to 85-90 °C. After sitting at the maximum temperature for 1 hour, the oven was reduced in temperature 10 °C every hour until room temperature was reached. Each piece was then carefully washed using soap and hot water.

The bioreactors both utilize a gas-permeable membrane backing which is comprised of Tegaderm (3M), a breathable, medical silicone laminated onto thin nylon mesh for structural support. The bioreactors were sealed against leaks using 0.5 mm

silicone rubber sheets, with two sheets used per bioreactor. Both the gas permeable membranes and the silicone were cut to the correct shape using the laser cutter. Figure 6 shows a 2D CAD model of the novel bioreactor, with each of the 5 laser cut components listed above and all relevant features labeled. The standard and novel bioreactors were held together using 7 and 8 (respectively) 4x16M bolts with one nut, two washers, and one spring washer each. A 5/8”x11 nut was affixed to the back of each system so that the systems could pair with existing bioreactor rotating driver systems. The acrylic piece described above was centered on the back plate and “welded” using methylene chloride. Contact cement was then used to hold the nylon nut in place on the acrylic piece.

All pre-tapped holes were then fitted with 1/4”-28 screw-to-male Luer adapters (McMaster-Carr) to hold all necessary components. Each bioreactor received two stopcocks (Cole Palmer) for filling and one standard cap for emptying and cleaning. All novel bioreactors were also given compression Luer fitting (Cole Palmer) to fill and empty the bubble catch channel.

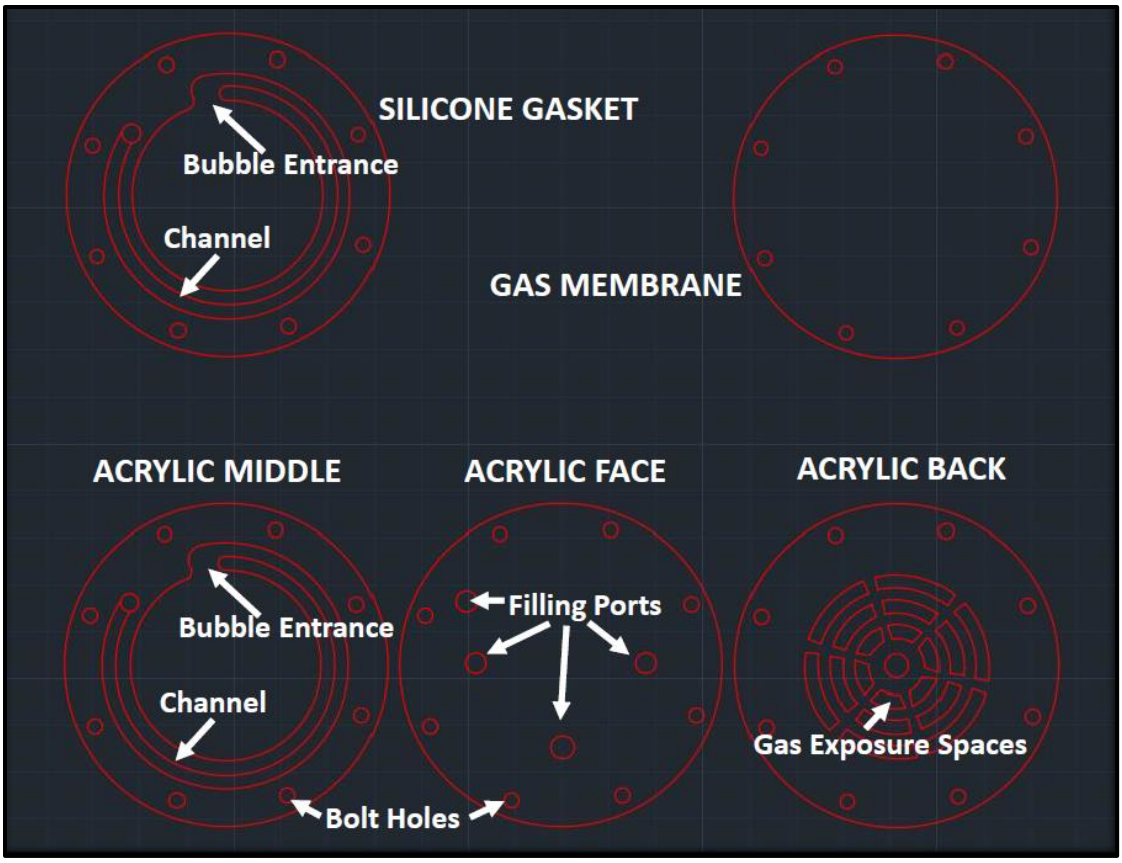

Figure 6: CAD Diagram of the novel bioreactor used for laser cutting. Appropriate labels have been added.

3.2. Aim 2

3.2.1. Validation of Fluid Dynamics Using Alginate Beads

In order to validate the modeled and simulated fluid dynamics from Aim 1, colored alginate beads were added to assembled bioreactors in water to visualize the motion of particles. Alginate was used due to its density near to cells and its tendency to form approximately spherical shapes when sodium alginate is dropped into calcium chloride solution. Four conditions were tested. First, the motion of beads in a completely filled standard HARV under ideal conditions; second, the motion of beads in a completely filled novel bioreactor; third, in a standard bioreactor with a small bubble present; and finally, in

a novel bioreactor with a small bubble present. Videos and pictures of the systems were taken while in motion over the course of 72 hours and evaluated for a host of qualitative factors. Because of the size of the particles and observed variation in densities between particles, the RWV system has to be run at a minimum of 15 rpm and some particle motion was present that would be unlikely in real cell culture. However, motion appeared near enough to approximations to provide a reasonable estimation of cell culture particle behavior.

3.2.2. General Cell Culture Methodologies

This section will describe the general cell culture methods used on all of the below experiments. Two types of cells were used. For spheroid and morphology studies, A549 Human Lung Cancer cells were used, as they rapidly form spheroids due to their high cohesion and ECM deposition characteristics and because they proliferate rapidly. Human Dermal Fibroblasts (HDFBs) were used for the cytotoxicity and channel capture experiments. The HDFBs, being a reasonably robust cell for non-cancerous cell lines, provide an acceptable metric for cytotoxicity. Additionally, the resistance to forming spheroids in the absence of scaffolding provides an ideal indication of single cell migration and fluid dynamics patterns. Both cell lines were cultured in complete DMEM (Corning, 10% Benchmark FBS, 1% Penicillin-Streptomycin (Gibco), 1% L-Glutamine). Media was changed every 2-3 days. Detachment of cells was performed by rinsing with DPBS and then incubating with Trypsin for 5 minutes. Cells were pelletized at 100 rcf.

Because both single cells and cell aggregates sediment over time, should cells be added to the novel systems and allowed to rest while the channel entrance is pointed down, over time cells will likely sediment into the channel and would be unlikely to return to the

main volume during culture. To prevent this, care was taken to ensure that when novel bioreactors were being handled, the channel entrance was always oriented upwards to prevent sedimentation. This extended the affixing of bioreactors to the rotary drive system and their removal. Effectively, the systems were either rotating or had their channels oriented upwards.

3.2.3. Bioreactor Sterilization and Conditioning

In every experiment in which bioreactors were used to culture cells, the same sterilization and conditioning protocols were used. These protocols were adapted from a 2006 Botta, et al. protocol paper describing the use an assessment of RWV bioreactors [64]. Although acrylic was determined to be the preferable cell culture material, it is prone to cracking and breaking when exposed to ethanol. Subsequently, ethanol was never applied directly to a bioreactor surface.

To sterilize, each bioreactor was first rinsed well three times with warm tap water. Next, each bioreactor was rinsed three times with sterile, autoclaved DI water. After rinsing, each HARV was filled completely with a 0.2 N NaOH solution (Fisher Scientific). Careful effort was taken to ensure that every port, stopcock, or opening used for each bioreactor was exposed to the solution and that any bubbles that would have prevented contact between the wall and the solution were removed. The HARVs were then covered and left at room temperature for a minimum of 24 hours. After 24 hours, the bioreactors were moved into a sterilized biosafety laminar flow hood containing a UV bulb. The fronts and backs of the bioreactors were exposed directly and closely to the UV light for a minimum of 15 minutes on each side. At this point through the completion of any experiment, the same syringe was never used to fill more than one bioreactor to prevent

cross contamination. The NaOH solution was then drained from the bioreactors and each was rinsed three times using 1x PBS (Gibco). At this point, the bioreactor was now considered sterilized and (typically) a conditioning step followed immediately.

Conditioning is a crucial step for each bioreactor, enabling blocking of protein binding surfaces and the prevention of cell-wall adhesion in what should behave as a suspension cell culture. First, a conditioning solution was produced. 50 mL of Benchmark FBS (Gemini Bio-Products) was added to 450 mL of 1x PBS (Gibco) at 7.4 pH and mixed well. 10 mL of Penicillin-Streptomycin (Gibco) was then added to the solution and mixed well. Although typical media will not exceed a 1% Pen-Strep concentration, the use of 2% Pen-Strep in the conditioning solution is intended to further decrease the probability of contamination from bacteria and should not affect cell culture performed with media at 1%. Each bioreactor was filled completely with the conditioning solution, with care taken to remove as many bubbles as possible. The bioreactors were then incubated for 24 hours at 37 °C on a 4RCCS System (Synthecon) rotating at 10 rpm. When cell culture was to begin, the conditioning solution was drained completely from the bioreactor and cells and media were added directly without rinsing.

3.2.4. Material Cytotoxicity Assay

In order to assess if proper cell culture experiments would have been affected by material composition, a cytotoxicity study was required. Although a typical cytotoxicity assay uses sensitive cells more prone to death, the scope of this study will not be to determine if the materials used are completely and 100% non-cytotoxic because, undoubtedly, materials used in commercial production are superior and, should this device be marketed, will be rebuilt with preferable materials. Instead, this assay will be performed

to determine strictly if the cell culture work to be performed in the bioreactor in the scope of this thesis might be negatively affected by the leaching of toxic chemicals from the materials. As such, of the two cell lines used (A549 and HDFB), it was determined that HDFBs, although reasonably hardy, were the more sensitive of the two and were thus used for the study.

On day zero, small pieces of each of the following materials were obtained: acrylic that has undergone laser cutting, plastic material from a stopcock, silicone rubber, Tegaderm, and nylon mesh. For solid materials 1-2 grams were used, while for flat materials ~2-4cm^2 were used. Each material was placed into separate 50 mL conical tubes (Falcon) and labeled appropriately. Each was rinsed well with several washes of 70% ethanol. A simplified version of the above sterilization protocol was implemented. Each tube was soaked in 20 mL 0.2 N NaOH for 2 hours, aspirated, then washed 3x with PBS, and exposed to UV for 30 minutes. 5 mL of DMEM was added to each tube and capped, then placed in a 4 °C refrigerator for 72 hours to allow leeching to occur along with 10 mL of control media containing no materials. Separate batches of DMEM were used for each replicate.

On day three, confluent HDFBs in T75s (Falcon) (passages 12, 16, and 20 for replicated 1, 2, and 3 respectively) were detached and resuspended at ~1 million cells per mL. 400 µL of each type of media were added to 3 wells each of a labeled 24-well plate. 6 wells were prepared of the control media for a total of 18 wells prepared per plate. ~100,000 cells (100 µL of suspension) were added to each of the wells excluding 3 of the control media wells. Plates were then incubated at 37 °C for 48 hours.

On day five, 50 µL of alamarBlue Cell Viability Reagent (Thermo Fisher Scientific) was added to every well starting left to right, top to bottom. The plate was then incubated for precisely 4 hours at 37 °C. After 4 hours, the plates were analyzed using a Tecan Infinite F200 Pro plate reader with a 545 nm/590 nm excitation/emission wavelength setting, 4 x 4 circular reading, 750 µm border, and no cover. A total of three replicates of this assay were performed.

3.2.5. Cell Culture for Validation and Morphological Assessment

Ultimately, the long-term objective of this thesis is to produce improved bioreactors for spheroid generation in RWV bioreactors and require validation with actual cell culture. While the presence of cells in a microgravity environment and in spheroids is known to result in changes of gene expression, the size and morphology of aggregates formed is considered sufficient evidence of fluid dynamics and cell culture behavior. Consequently, PCR or other techniques for evaluating gene expression were not employed. The experiment for this section, the cell culture of A549 cells for the purpose of evaluating spheroids while under bioreactors, were performing under ideal conditions with no bubbles present in the standard bioreactors and only small incidental bubbles in the novel designs. Of note, great care was taken during this experiment to remove as many bubbles from the systems of the standard bioreactors as possible while similar care was not taken with the novel designs. This was for two reasons: first, by their design, even a small incidental bubble would still represent ideal conditions in the novel bioreactors; and second, because the novel designs are expected to increase ease of use, not bothering with the extensive bubble clearing and prevention required of the standard designs was a necessary omission to evaluate handling difficulty.

On day zero, A549 Human Lung Cancer Epithelial Cells (Passages 55 through 62) were brought to confluence in T-75 cell culture flasks (Falcon) and then detached and resuspended at between 1,500,000 and 2,000,000 cells per mL. Properly sterilized and conditioned standard and novel bioreactors were drained of conditioning solution and had about 3 mL of warmed complete DMEM (Corning) added to the main volume of each. 1 mL of the A549 cell suspension solution was then added to each system through the main filling/emptying port. Prior to each of the 1 mLs of cell solution being drawn, the tube containing the cell solution was turned several times to ensure mixing. For the standard bioreactors, the main filling port was closed and a syringe of DMEM was connected to one stopcock while the opposite was left open. A small volume was aspirated until the air in the top of the stopcock was cleared. Media was then added to the bioreactor until the system was completely cleared and a small amount of media was ejected through the opposite stopcock. Both stopcocks were closed and the bioreactors were turned, flipped, and gently tapped to encourage any remaining bubbles out. Invariably, new bubbles appeared and were cleared by displacing them using the same syringe-stopcock method prior to incubation. For novel bioreactors, one stopcock was left open while the filling port and the other stopcock was closed. The syringe with DMEM was then connected to the compression fitting at the end of the channel perimeter. DMEM was then added through the port until the system was completely filled with media. No great effort was taken to clear all bubbles. Once all bioreactors were filled, they were fitted to the 4RCCS (Synthecon) motorized driver system running at 10 rpm and incubated at 37 °C for 72 hours.

On day three, all bioreactors were removed from the 4RCCS. The novel bioreactors were removed by waiting until the rotating oriented the channel entrance upwards; the bioreactor was then held and unscrewed by turning the male screw connector of the 4RCCS. Bioreactors were then moved to a sterile laminar flow hood and aggregates were allowed to settle for ~5 minutes. After settling, one stopcock was opened and the main fluid bodies of both types of bioreactors were moved into labeled 15 mL conical tubes (Falcon). For the novel designs, the remaining 2.5-3 mL was collected through the channel port into a separate 15 mL tube. All aggregates in the tubes were allowed to settle for ~3-5 minutes until all visible aggregates had settled to the bottom of the tube. For tubes containing media volumes exceeding 3 mL, media was aspirated until ~3 mL remained. 1000 µL pipette tips had ~1 cm cut off using scissors to increase the cross-sectional diameter of the tip. 300 µL was then extracted from the bottom of the tubes to ensure all aggregates were collected. The volumes were deposited on MatTek dishes that had been treated with poly-L-lysine to increase adhesion. Multiple images were then captured using phase microscopy at various magnifications. Aggregates were then treated with 300 µL of 3 µM Calcein AM and 300 µL of 3 µM of Propidium Iodide consecutively for 30 minutes each, for fluorescent staining for later confocal microscopy.

3.2.6. Intentional Addition of Bubbles with Cell Culture

While the previous experiment was intended to demonstrate the capacity for both the standard and novel systems to produce spheroids under ideal conditions, the purpose for designing the novel bioreactor was to ensure protection and stabilization of the necessary fluid dynamics of these systems while under non-ideal conditions. To that end, it became necessary to intentionally induce the most common failure mode of the RWV

and purposefully inject moderately sized bubbles into the bioreactors. The effects of disrupted fluid dynamics on spheroid formation in the standard bioreactors and the capacity for the novel designs to prevent that disruption were then analyzed. Importantly, the results of this experiment were compared directly to the non-bubble culture morphology experiment described above. Because of that, the bubble injection experiment was performed as a slight modification to the general culture morphology experiment.

In order to perform the bubble injection experiment, the same A549 cells, same cell concentrations, and same volumes were used as the previous experiment. The distinguishing feature of the bubble injection experiment is that after the complete filling of the bioreactors in order to remove all bubbles, a second syringe containing only air was connected to one of the stopcocks and a small bubble of air, between 250 µL and 500 µL, was added. Because the stopcock itself contains a small volume of media, that volume has to be displaced before a bubble can be properly measured and added. This difficulty contributed to the large range of air bubble volumes and was the reason substantially smaller air bubbles were not attempted. After the air bubbles were added, the bioreactors were incubated under standard conditions for 72 hours and analyzed in a similar capacity to the general cell culture morphology experiments.

3.2.7. Channel Capture of Cells

Of all potential failure modes likely to occur in the novel bioreactor design, one of the most concerning is the possibility of cells migrating into the channel during cell culture as a result of gravity due to sedimentation, centrifugal force, or net flow in the channel. Should this failure mode be highly probable, and because objects entering the channel are unlikely to leave it, the net effect could be that near 100 percent of cells added to the system

are caught in the channel. Cells in the channel would experience high interactions with the walls, high shear, and likely would not be exposed to simulated microgravity. Consequently, it becomes necessary to assess the probability of that migration happening. Based on the mathematical and CFD results to be discussed below, it was determined that cell migration to the channel was most likely to occur before inertial equilibrium had fully established a solid body state. As this is estimated to take somewhere from the minutes to hours range, it was decided that only a single, 24-hour time point was required to reasonably describe the "channel capture" failure mode. Low cell concentrations were used in this experiment to further decrease the probability of aggregates forming and skewing the results.

To perform this experiment, sterilized and conditioned novel bioreactors were filled with approximately 3 mL of warm DMEM into the main body. HDFBs (P 15, 16, 18) were detached from their flasks and resuspended at a concentration of ~100,000 cells/mL. 500 µL of cell suspension were added to each of the novel bioreactors and the systems were filled completely with DMEM through the compression Luer fitting on the channel port. Particular care was taken during filling to prevent backflow or sedimentation of cells into the channel. As with the morphology experiments, effort was not taken to clear all bubbles from the system and as a result, small bubbles were present in every bioreactor that ran this experiment. Each bioreactor was incubated at 37 °C for 24 hours at 10 rpm on that 4RCCS system. After incubation, volumes from the main body and from the channel volume were collected into separate 15 mL tubes. The tubes were then centrifuged at 150 rcf and resuspended in 1 mL of warm DMEM. Cell counting was performed using a hemocytometer. Three measurements were taken from each 1 mL sample to ensure

accuracy and each tube was vortexed for ~2 seconds before samples were drawn to ensure volumes were properly mixed.

3.3 Statistics

All experiments evaluated statistically were replicated a minimum of three times. Randomization was ensured by satisfying at least three of the following conditions between replicates: experiments performed on different days, with different passages of cells, using different batches of media, using different bioreactors, and running the systems on separate 4RCCS devices. All error bars shown indicate standard deviation unless otherwise stated. Significance was evaluated using a two-tailed student t-test. Experimental results are considered significant only if the p value is less than 0.05.

CHAPTER 4

RESULTS

4.1. Aim 1

4.1.1. Mathematical Modeling

First, a simplified model of fluid dynamics disruption and shear stress due to bubble interference will be discussed. Because this is a significantly simplified model, several assumptions must be made. First, due to buoyancy, the position of any bubble will always be fixed to highest point of the vessel relative to the ground. Next, the bubble will be completely round. Also, because a turbulent system will likely have a higher net shear than a stable system, solving these systems in laminar models will represent shear minimums. Finally, because the distance between the wall and the particle is zero, the shear approaches infinity, a minimum distance between a particle and a relatively stationary body (either a bubble or a wall) will be estimated at 100 micrometers. In practice, this height value may be lower, so shear estimations could be higher than estimated values. Figure 7 shows the expected path of a particle over time (shown in black) as it rotates counterclockwise in a moving bioreactor and encounters a bubble. In this ideal system, the bubble follows the path of rotation, until it is forced to deflect around the bubble, experiencing a change in velocity relative to the fluid of zero (when in solid body motion) to the opposite velocity of the rotation of the bioreactor. At the lowest possible distance, the particle will "contact" the bubble for about half the 2D perimeter of the bubble. The equation shown in Figure 8 shows the equation used to calculate fluid shear stress on any surface [65]. Assuming standard conditions of 10 rotations per minute ('V' is approximately 2.6 cm/second), a fluid dynamic viscosity of 0.01 dyne seconds per centimeter squared, and a bubble volume

of just 100 microliters, the calculated shear stress would equal about 2 dynes per square centimeter and would scale rapidly with bubble volume.

This value of 2 dynes per square centimeter is representative of a shear stress experienced in an average vein and would be substantially detrimental to aggregate formation [66]. The subsequent turbulence would also result in a loss of the roundness of the path of rotation of the bead, negating microgravity simulating effects. Additionally, the deflection would then proliferate to multiple fluid shells beyond the vertical diameter of the bubble, disrupting the microgravity environment for more particles than just those interacting with the bubble. Because shear is effective a measure of pressure, the pressure found at the particle surface is offset by a negative pressure that forms behind the bubble. The eddy current that subsequently forms induces turbulent mixing for the entirety of the system that could increase shear for all particles. Fundamentally, this model demonstrates that even a small bubble, representing just 1% of the total volume of the bioreactor, can have devastating effects.

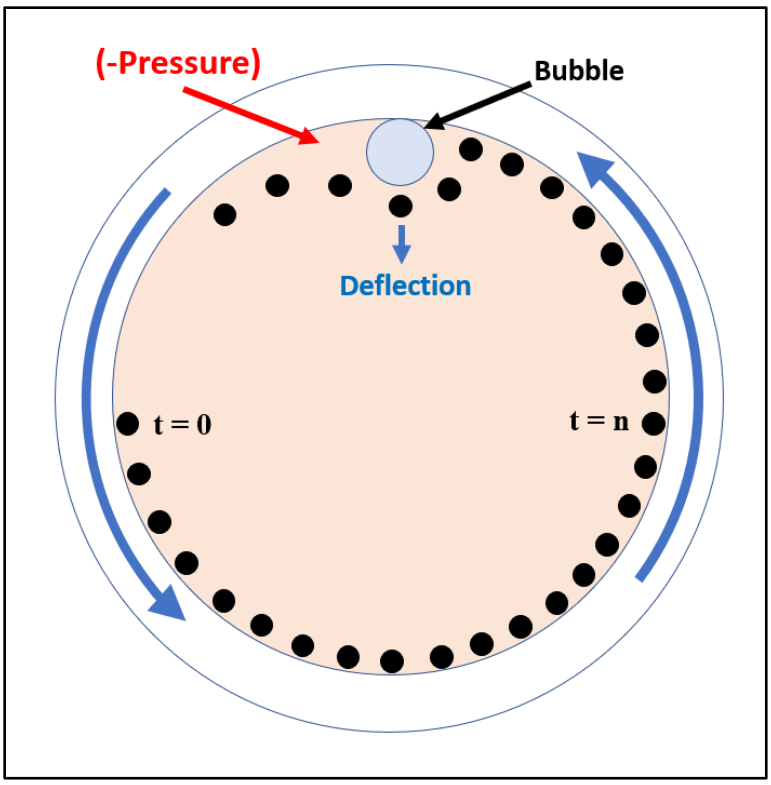

Figure 7: Model of particle motion (black) in a standard HARV around a bubble.

$$\tau = \frac{-8 * \mu * V * du}{(dy)^2}$$

τ = Shear Stress, μ = Dynamic Viscosity, V = Velocity,
du = Distance Traveled, dy = Height Between Surfaces

Figure 8: Shear stress equation. dy is determined by the distance between a particle and the bioreactor wall. [65].

With the severity of the bubble interference described, a generalized description of a bubble removing modification can now be defined. Such a modification must possess several key properties. The modification must be capable of constantly removing bubbles from the circular body of an RWV without changing the body's inherent shape, it must prevent bubbles from reentering the system, and the modification must be connected to the main body of the RWV in a such that there is unbroken fluid contact between the sections.

In pursuit of realizing these properties, the unidirectional rotation of the RWV and the buoyancy of air in a liquid were each leveraged. Because an air bubble will always rise to the topmost wall of the RWV and because rotation ensures the entire wall will be exposed to that bubble in each rotation, the modification must have an opening or "entrance" at the fluid-wall boundary. Additionally, because a bubble will only continue to rise through a liquid when displaced by another liquid, the modification must contain that fluid. Finally, because a bubble released from the bottom of a circular container of fluid will rise to a position 180° from the point of release, if a bubble is "released" from the segregating modification at a distance more than 180° from the point of the "entrance" then the bubble cannot reenter the main circular body of the RWV. With these concepts in mind, a potential modification can be described as a small entrance at the wall of the RWV that leads to an extended, thin channel in a concentric but isolated arc along the majority of the perimeter of the body running in a clockwise direction. One such modified RWV is shown in Figure 9 and Figure 10 which demonstrate how a bubble may behave in an idealized rotating channel with a back wall. Such a design would positively separate and permanently isolate bubbles from the main volume of the RWV system.

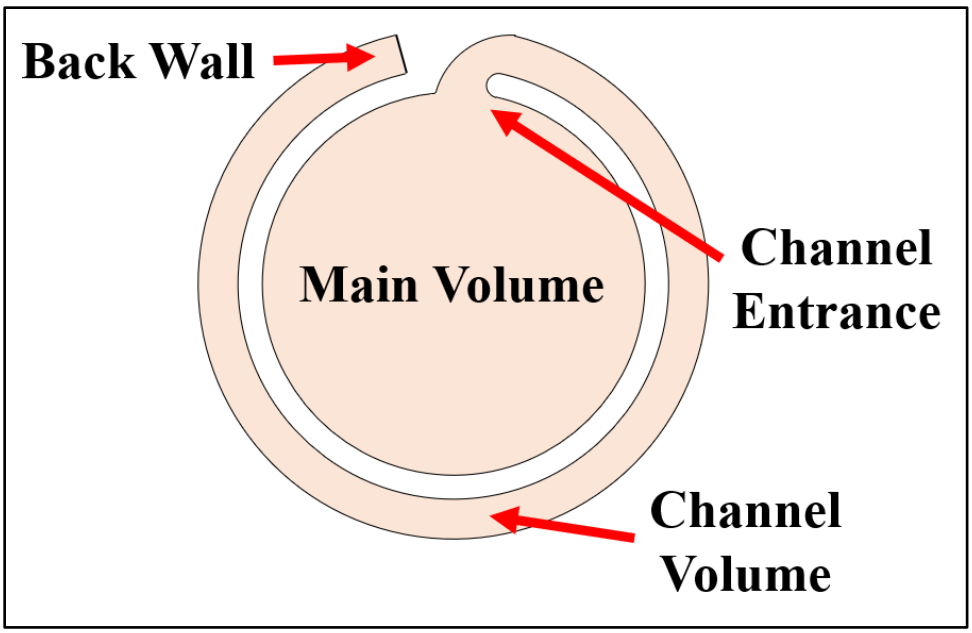

Figure 9: A diagram of one novel RWV modification capable of separating bubbles.

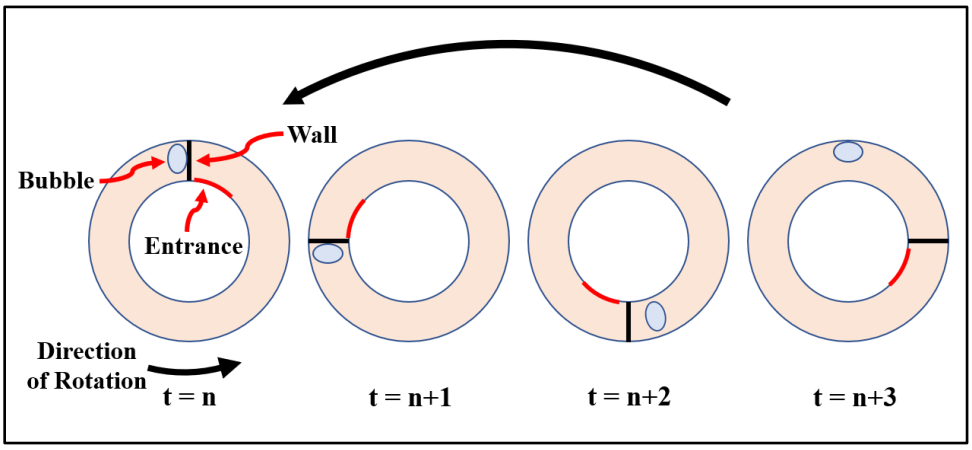

Figure 10: State diagram of bubble motion in a rotating walled channel. The bubble cannot re-approach the channel entrance. The timepoints show and arbitrary time to complete on rotation.

With a potential bubble removing channel, as described, it becomes necessary to estimate if such a RWV modification would interrupt or disrupt the solid body rotation it was intended to protect. To that end, a model of the flow in the bubble removal channel and the entrance to that channel was modeled. As discussed in the introduction of this thesis, when a cylinder completely filled with an incompressible fluid begins to rotate along its axis, the bulk of the fluid will not instantaneously begin to act as a solid body. However, if that rotation were occurring in the xy-plane and the cylinder began to move in a straight line along the z-axis, solid body motion will begin immediately in that straight line [53]. This is due to the bulk of the fluid interacting with the base of the cylinder and exerting an equal and opposite force on the base of the force inducing the linear motion. This same concept can be used to estimate the behavior of fluid in the channel of the modified RWV. Because there is a "wall" in the back of the channel, as rotation initiates, a force proportional to the velocity of the rotation times the mass of the fluid in the channel will be applied on the back wall as shown in Figure 11. Subsequently, the fluid in the channel will be expected to act as a solid during rotation and will not contribute to net flow.

With most of the channel immediately exhibiting a solid body state during rotation, the majority of the channel can be excluded from our modeled description of flow around the entrance to the channel. The portion retained in our model is shown in Figure 12. While the bulk of the channel is excluded, the fluid dynamic viscosity at the entrance to the channel inducing less drag relative to the no-slip condition of the wall-fluid interface is expected to increase the time to complete solid body rotation. However, as long as the fluid in the entrance to the channel continues to exist in a linear solid body condition, the slowed

fluid velocity in the direction of rotation around the entrance will not prevent the formation of complete solid body rotation but will simply increase the time until fluid equilibrium is established.

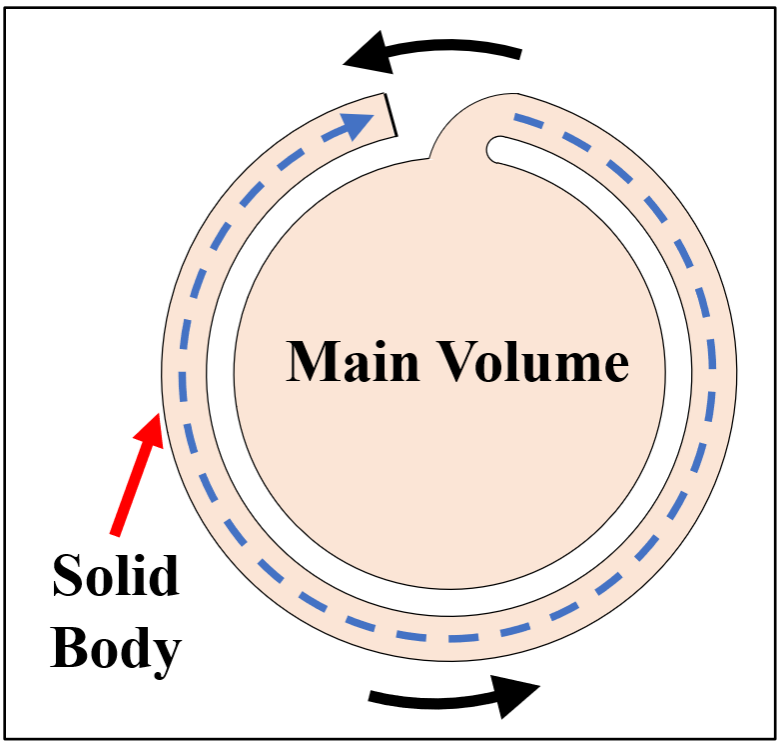

Figure 11: The expected linear solid body condition in the fluid of the bubble removing channel. Black lines indicate direction of rotation.

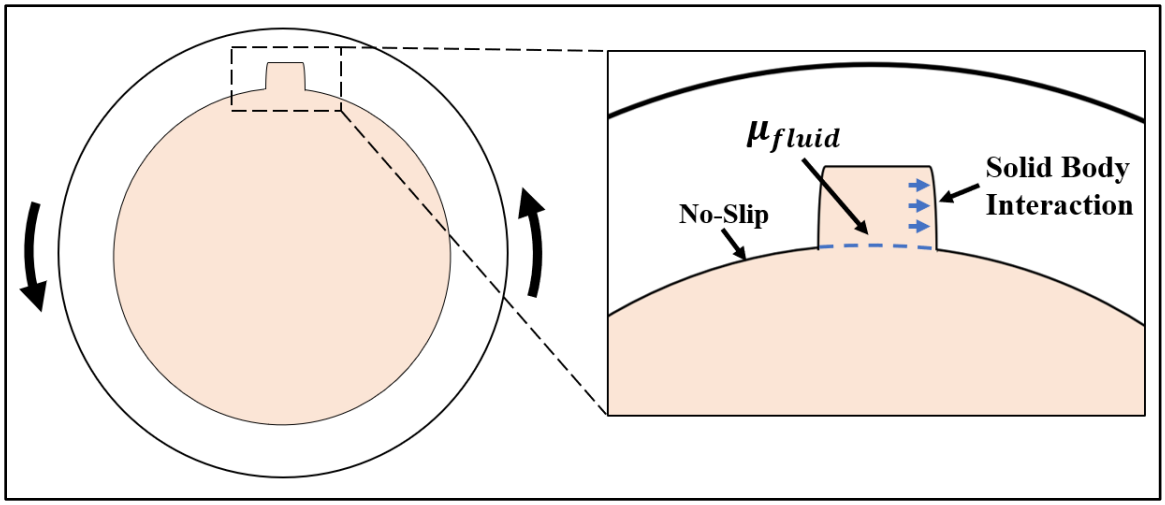

Figure 12: The simplified model of fluid interaction at the entrance to the bubble removing channel of the modified RWV.

4.1.2. Computational Fluid Dynamics (CFD)

After CFD simulations were run in Fluent, stable animations were produced of the 2D fluid velocity vectors over time of both a standard RWV and one containing the novel design described in this thesis. Figures 13 and 14. demonstrate the velocity vectors in the standard bioreactor after less than one second of run time, and after 3 minutes, exhibiting inertial equilibrium. Figures 15 and 16. show the same time points for the novel design. The velocity magnitude scale bars on the left demonstrate approximately the same range. Note, the same approximate velocity vectors appear, in the same circular pattern, extending through approximately the same distances of each bioreactor. This is an indication that ideal solid body rotation can indeed be established in the novel bioreactor designs. There is a slight drop-off of velocity at the exact entrance to the channel, but it is quickly rectified when the wall is reencountered and closely resembles the expected flow as defined in the mathematical model. Furthermore, only slight fluid motion, near an order of magnitude less than in the main body, is present in the channel and this flow is consistent and unchanging between one second and three minutes. These all provide reasonably strong indications that the novel design, at least theoretically, should behave as expected. Attempts to introduce air bubbles to this simulation were unsuccessful as stability for either system decayed, and the animations, even for the standard design, appeared closer to an emulsion rather than actual bubble behavior. However, the bubble behavior will likely be able to be observed much more realistically in physical experiments in the next aim.

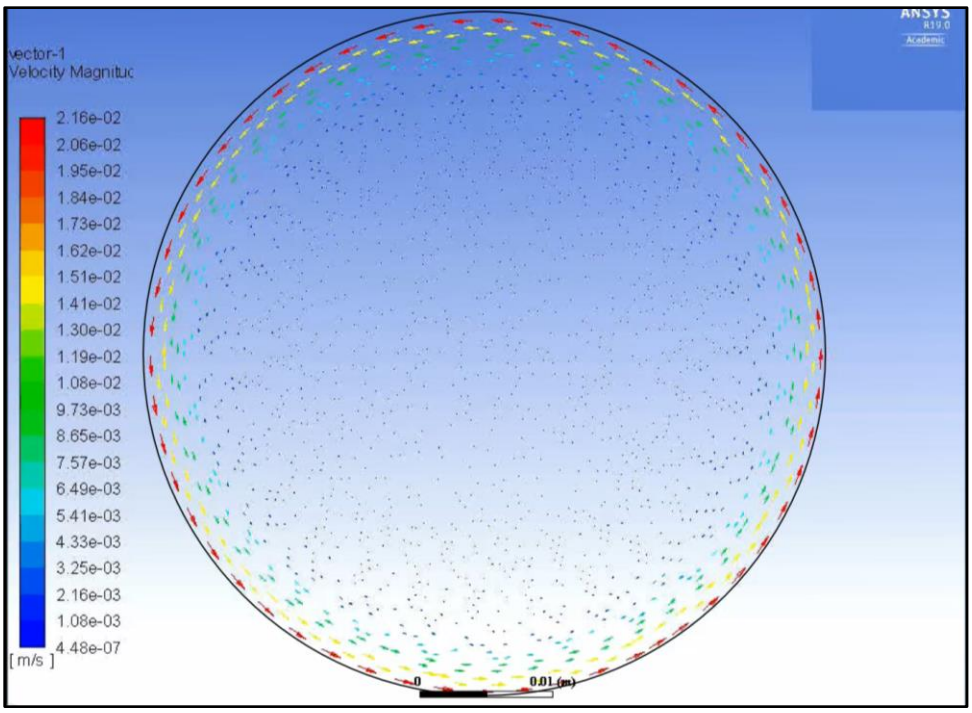

Figure 13: 2D simulated fluid velocity vectors in standard design RWV at approximately 1 second after start-up.

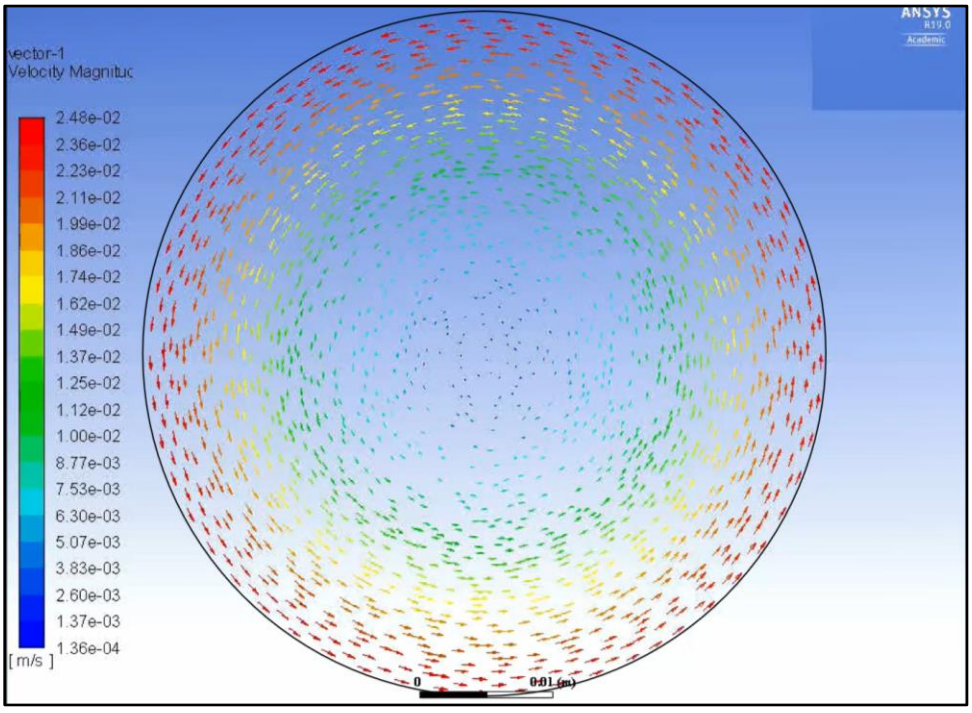

Figure 14: 2D simulated fluid velocity vectors in standard design RWV at approximately 3 minutes after start-up.

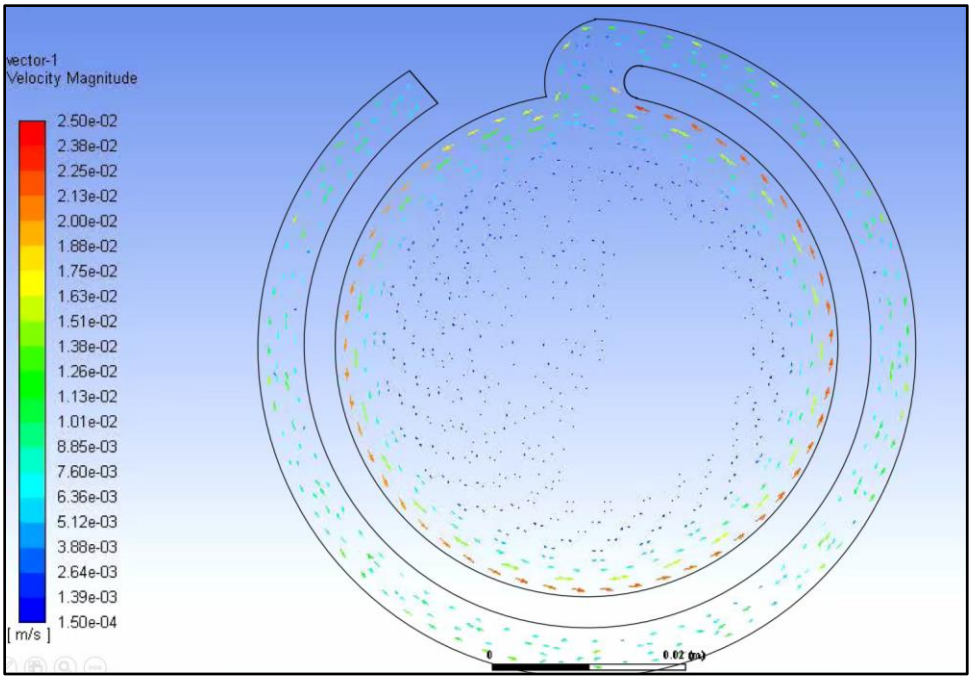

Figure 15: 2D simulated fluid velocity vectors in novel design RWV at approximately 1 second after start-up.

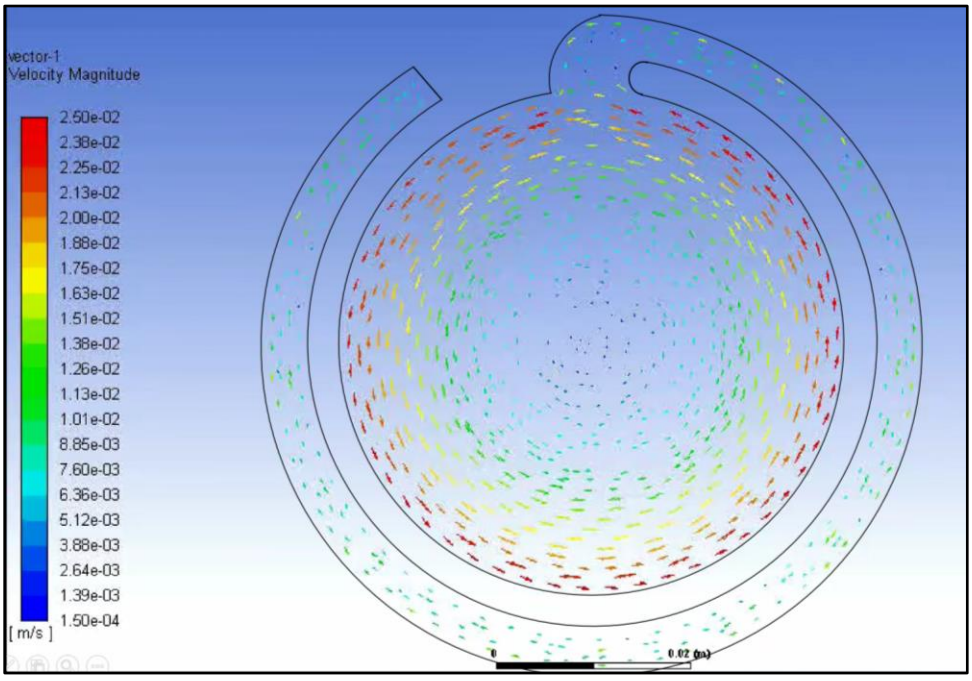

Figure 16: 2D simulated fluid velocity vectors in novel design RWV at approximately 3 minutes after start-up.

4.1.3. Bioreactor Design and Fabrication

With mathematical and computational modeling indicating the feasibility of the bubble separating channel, a design phase must plan key requirements, fabrication techniques, and dimensions to be used for the translation of the modified RWV into a finished prototype of the novel design. Additionally, it is necessary to design and build an RWV replicating existing commercially available HARVs using the same materials and techniques as those employed in the novel HARV so the most direct comparisons can be made. These two designs will be referred to as the novel design HARV and standard design HARV respectively.

First, there are several critical requirements that a finished bioreactor must take into account. Because these HARVs will eventually be used for cell culture, all materials used which will come into contact with cells or media must be able to be sterilized and would be expected to be non-cytotoxic. Towards that end acrylic, rubberized silicone sheets, medical grade stopcocks, and Tegaderm (3M) were chosen for construction. Additionally, all of the sheet materials must also be capable of being laser cut. In addition to being useable for cell culture, these devices must be as leak proof as possible to prevent new bubbles from entering the system and will thus be constructed with nuts and bolts to ensure high, even pressure will hold all the components together. Filling ports were added to all positions found on commercially available vessels along with the back wall of the channel.

Finally, the dimensions of both the materials and final devices must be outlined. Table 1 shows the dimensions of the materials used and the final structures of the standard and novel design HARV. The fully constructed devices are shown in Figure 17, filled with media to demonstrate the fluid volume of each system.

Design	Dimension	Value
Materials	Acrylic	3/16”
	Silicone	0.010”
	Bolts and Nuts	4x16M
Standard HARV	Total Volume	~10 mL
	Inner Diameter	5.1 cm
	Outer Diameter	7.6 cm
	Number of Bolt Holes	7
Novel HARV	Main Volume	~10 mL
	Channel Volume	~2.5 mL
	Inner Main Diameter	5.1 cm
	Inner Channel Diameter	5.9 cm
	Outer Channel Diameter	6.7 cm
	Outer HARV Diameter	8.8 cm
	Channel Entrance Width	7 mm
	Channel Length	18 cm
	Number of Bolt Holes	8

Table 1 – List of dimensions used in the design of standard and novel HARVs.

Figure 17. – The fabricated novel (left) and standard (right) HARVs filled with media.

4.2. Aim 2

4.2.1. Validation of Fluid Dynamics Using Alginate Beads

Images and videos of both the standard and novel HARV running after several periods of time were taken. For the sake of this thesis, three conditions with special significance to the above models and designs will be discussed. The three conditions are the behavior of alginate beads in a standard design with a bubble after 1 hour, the behavior of the beads in the novel design without a bubble after 48 hours, and the behavior of the beads in a novel design with a bubble after 24 hours. Sets of two still images will be presented to indicate the passage of time between frames of a video over the stated period of time.

First, the motion of alginate beads around a small bubble in standard HARV. Figure 18 shows the motion of alginate bead around a very small (~5 mm diameter) bubble in less than 1 second, an approximately 60° turn. Note, how through interaction with the bubble, the three beads, labeled “A”, “B”, “C” move from a linear arrangement to a triangular one. The motion of the bead “C” in this image represents a change of approximately 1 cm in 0.9 seconds. This motion, even while omitting surface velocity due to rotation or fluid turbulence, represents a minimum relative velocity of particle “C” to particle “B” of 0.011 meters per second which, in the first frame, start approximately 1 mm apart according to the scale bar. Applying those values to existing fluid shear equations as shown in Figure 8 give an approximate shear stress level of 8.8 dynes per centimeter square at a minimum, which, is just shy of the shear experienced in a small artery [66].

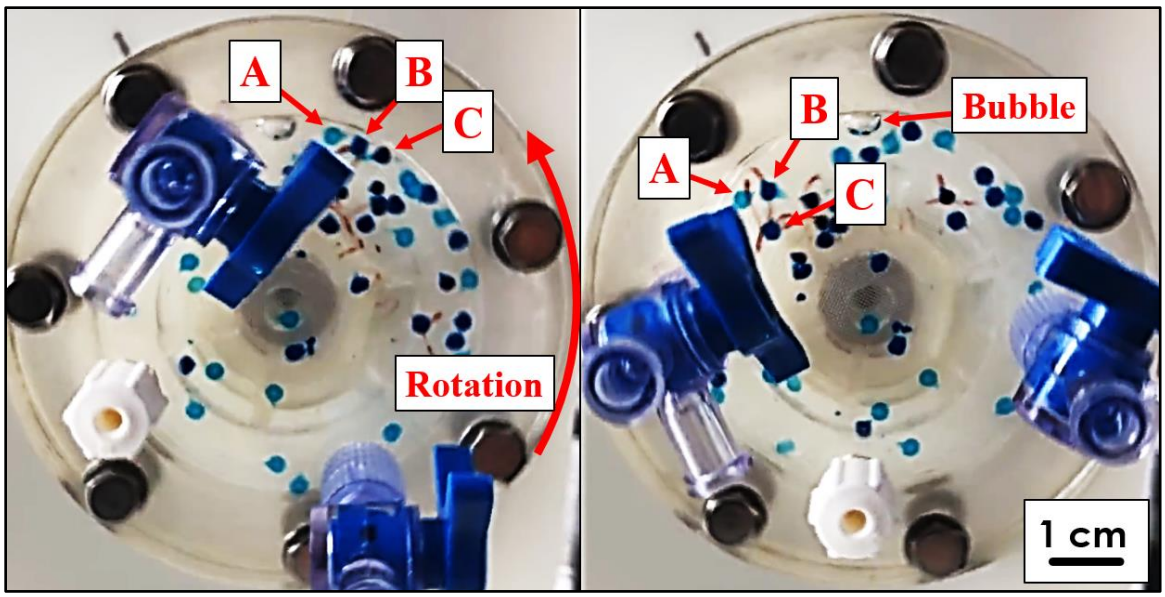

Figure 18: Two frames of alginate beads in a standard design HARV encountering a small bubble over ~1 second. Beads A, B, and C, represent the same beads in each image.

Second, the behavior of alginate beads in a novel HARV after 48 hours. This timepoint was selected to demonstrate a stabilized fluid dynamics system and to consider the probability of beads erroneously migrating to the channel over the main volume. An image of a full rotation of this setup is shown in Figure 19. While one bead "F" has fully entered the channel and another is tending that way, the vast majority of the beads remain in the main body. Furthermore, looking at beads "D" and "E", over the course of one full rotation, very little net motion is observed relative to other alginate beads.

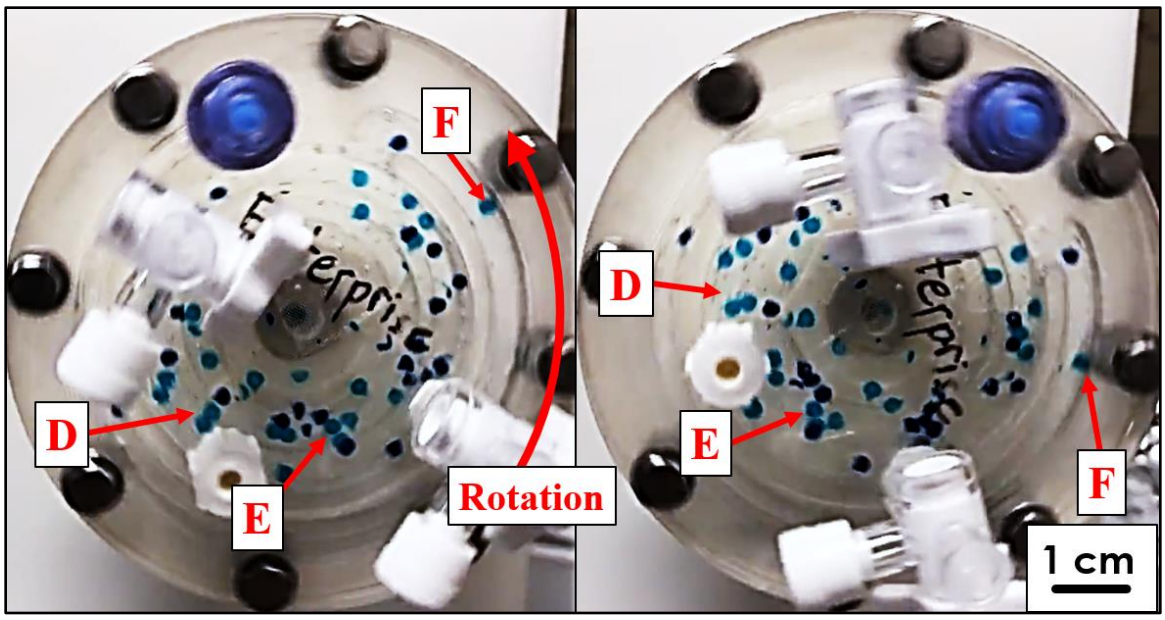

Figure 19: Two frames of alginate beads in a novel design HARV without a bubble over ~3 seconds after 48 hours. Beads D, E, and F, represent the same beads in each image.

Finally, Figure 20 shows a similar setup to the above example, but with a substantial bubble added. Again, as seen with the previous example, very little net motion is seen between beads “G”, “H”, and “I”. This study demonstrates that solid body rotation is still capable of being sustained in the novel design even with the presence of a bubble.

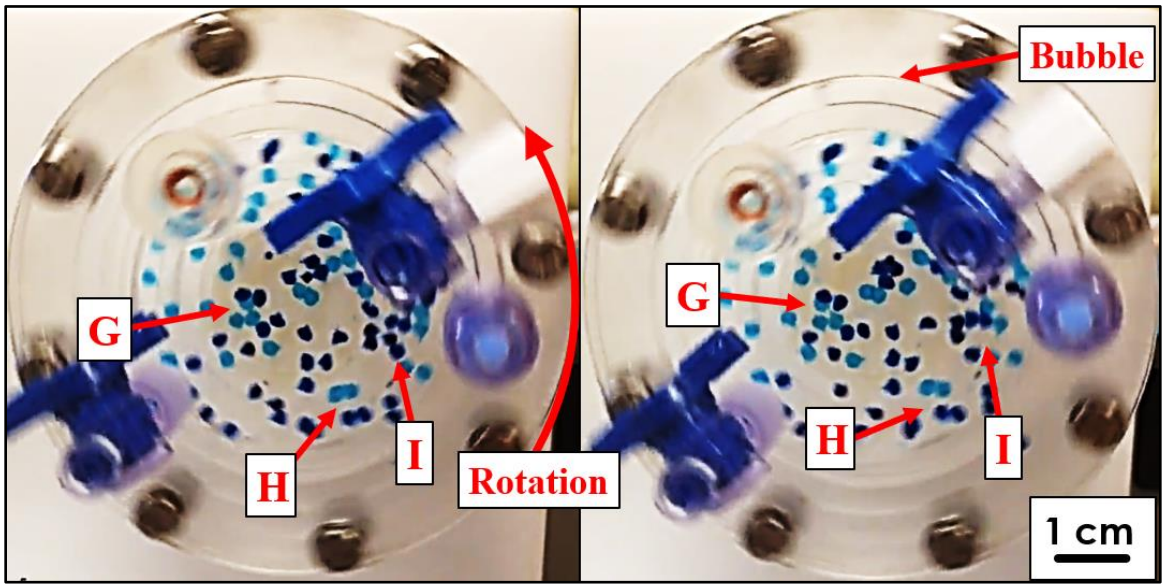

Figure 20: Motion of beads in a novel HARV with a bubble segregated in the channel.

4.2.2. Material Cytotoxicity Assay

The alamarBlue assay is a measurement of metabolic activity. The degree of fluorescence measured at 590 nm is a direct representation of the amount of metabolism occurring in the cell and is subsequently a strong indicator of cell health and viability. The measured fluorescence of each replicate is shown in Figure 21. There is no statistically significant difference between any of the material samples and the positive control. This is compared to the extremely significant ($p<0.0001$) difference between any of the samples and the negative control containing no cells. This strongly indicates there is no measurable cytotoxic effect of any of the selected materials in the bioreactor fabrication.

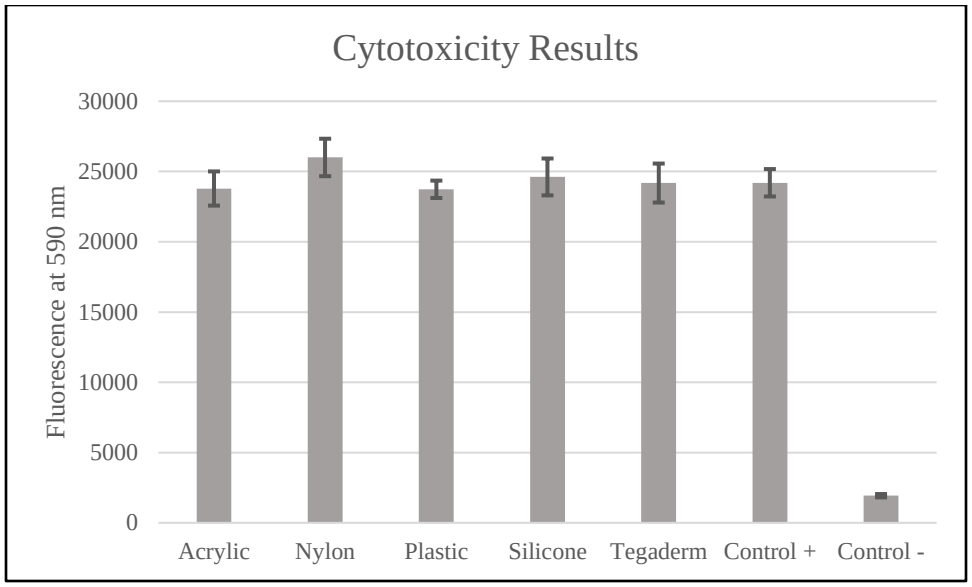

Figure 21: Cytotoxicity results. No significance between any of the materials tested and the cell positive control (min p-value of 0.1013). Substantial significance between all cell containing tests and the negative control (max p-value <0.0001).

4.2.3. Cell Culture for Validation and Morphological Assessment

As stated in the introduction of this paper, it is extraordinarily difficult to prevent bubble formation in standard HARVs, consequently, results from several replicates from the standard HARV group had to be excluded from this study due to bubble formation and subsequent disruption. For all images taken from the bioreactors that did not experience a bubble failure, ImageJ analysis was performed by manually outlining the perimeters of all major aggregates visible in each image and collecting data on area and circularity. Confocal images were kept purely for qualitative analysis due to poor penetration of light through the spheroid body. While the below images represent two of several hundred analyzed, they provide a clear indication of the novel bioreactor design's capability to reproduce spheroids of remarkable similarity in size and morphology to those of the standard design. Figures 22 and 23 show representative images of spheroids gathered through the standard design bioreactors and novel bioreactors respectively.

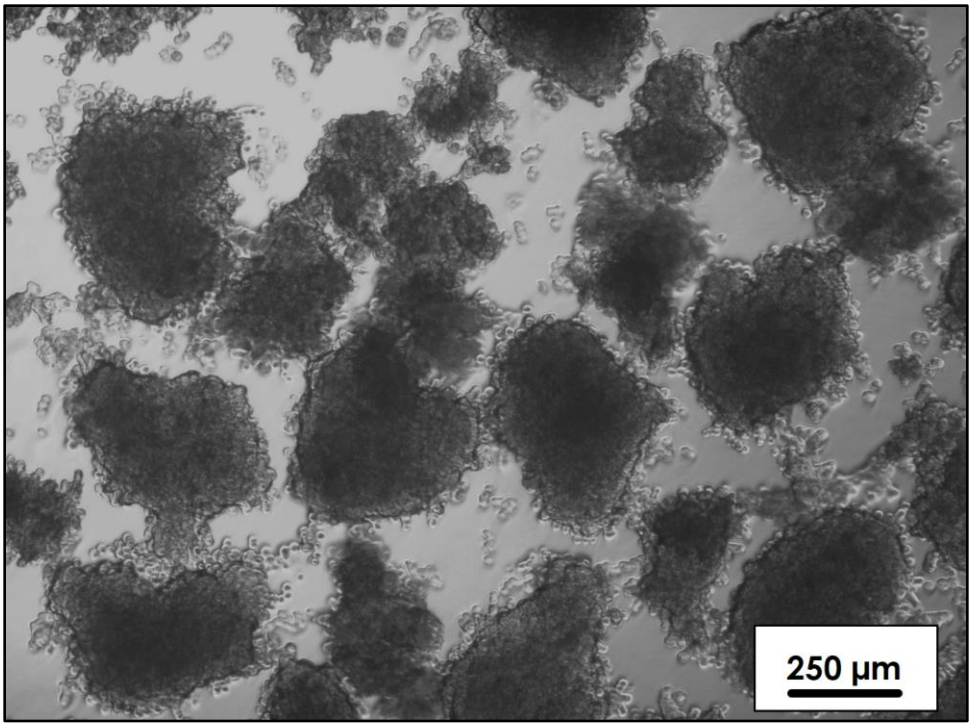

Figure 22: Spheroids formed under ideal conditions in the standard design HARV.

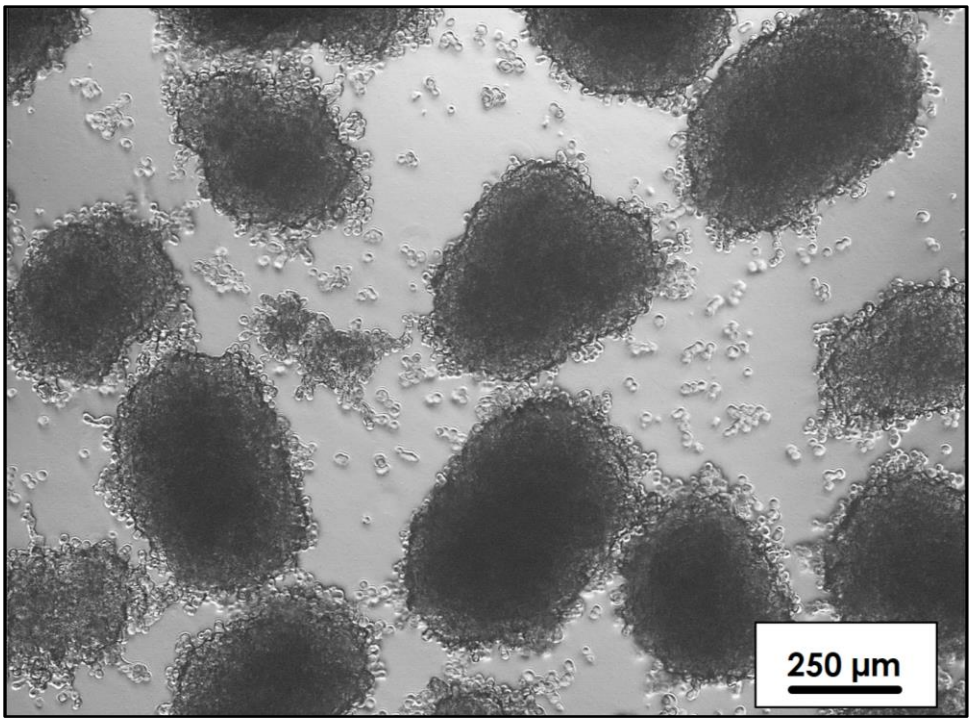

Figure 23: Spheroids formed under ideal conditions in the novel design HARV.

For quantitative analysis of spheroid size and morphology, some data processing was required. Because of outliers due to small aggregates that were unable to grow or so-called “aggregates of aggregates”, masses of aggregates that group into larger structures, there was a large standard deviation within replicates. As such, medians of spheroid size were taken of individual replicates. All replicates of a single group were then averaged and the standard deviation of those averages was taken. The data is shown in Figure 24. Although there is still a reasonably high standard deviation, the data demonstrates there is no significant difference is the area of spheroids generated in the two types of bioreactors when run under ideal conditions. Figure 25 shows the circularity averages of the same images. Figure 26 shows an example of a fluorescent confocal microscopy image taken of one spheroid. Green is Calcein AM and signifies alive cells while red is Propidium Iodide and signifies dead or dying cells.

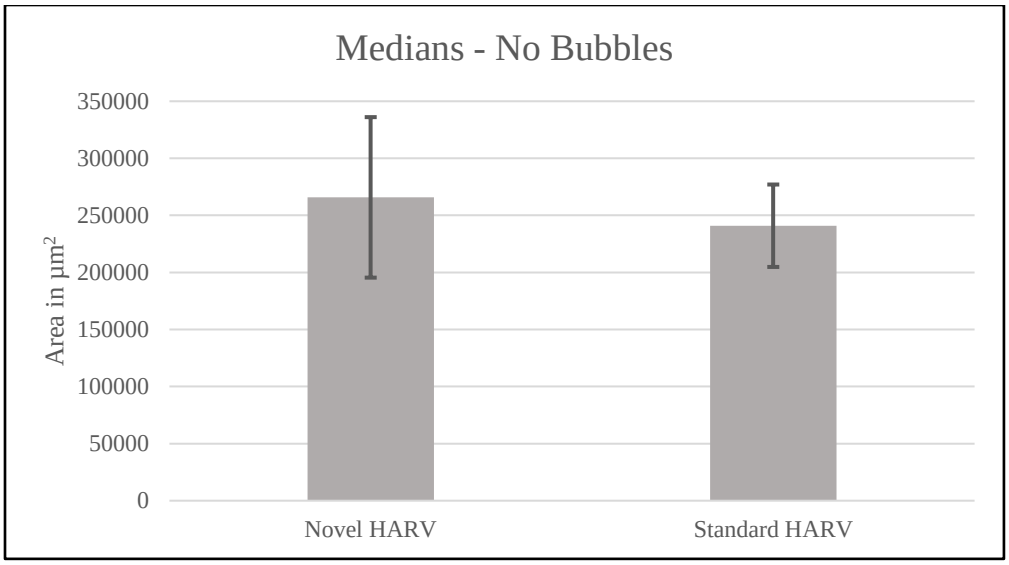

Figure 24: Average of medians of area in micrometers squared in novel and standard design HARVs cultured in ideal conditions. The difference is not statistically significant with a p-value of 0.6055.

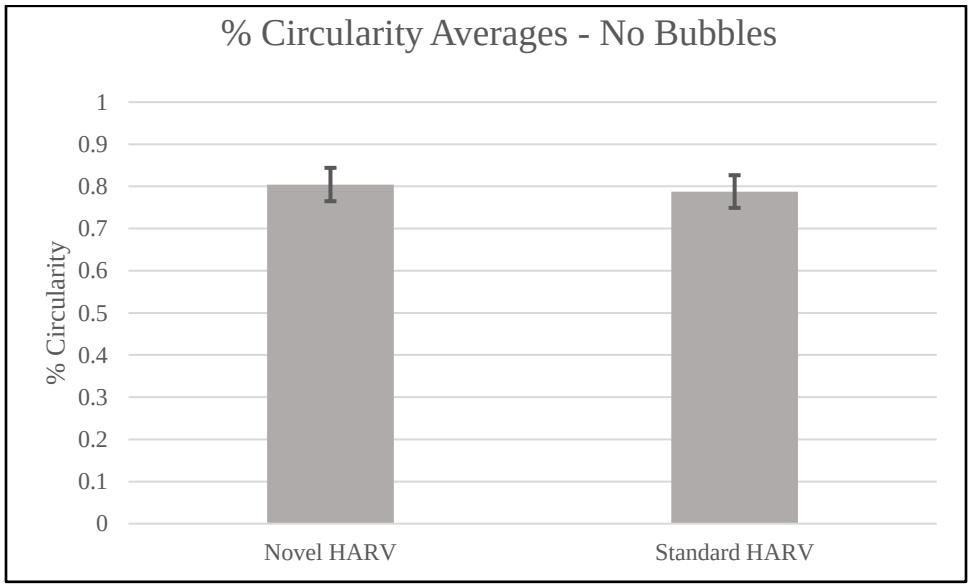

Figure 25: Average of averages of circularity of novel and standard design HARVs cultured in ideal conditions. The difference is not statistically significant with a p-value of 0.5290.

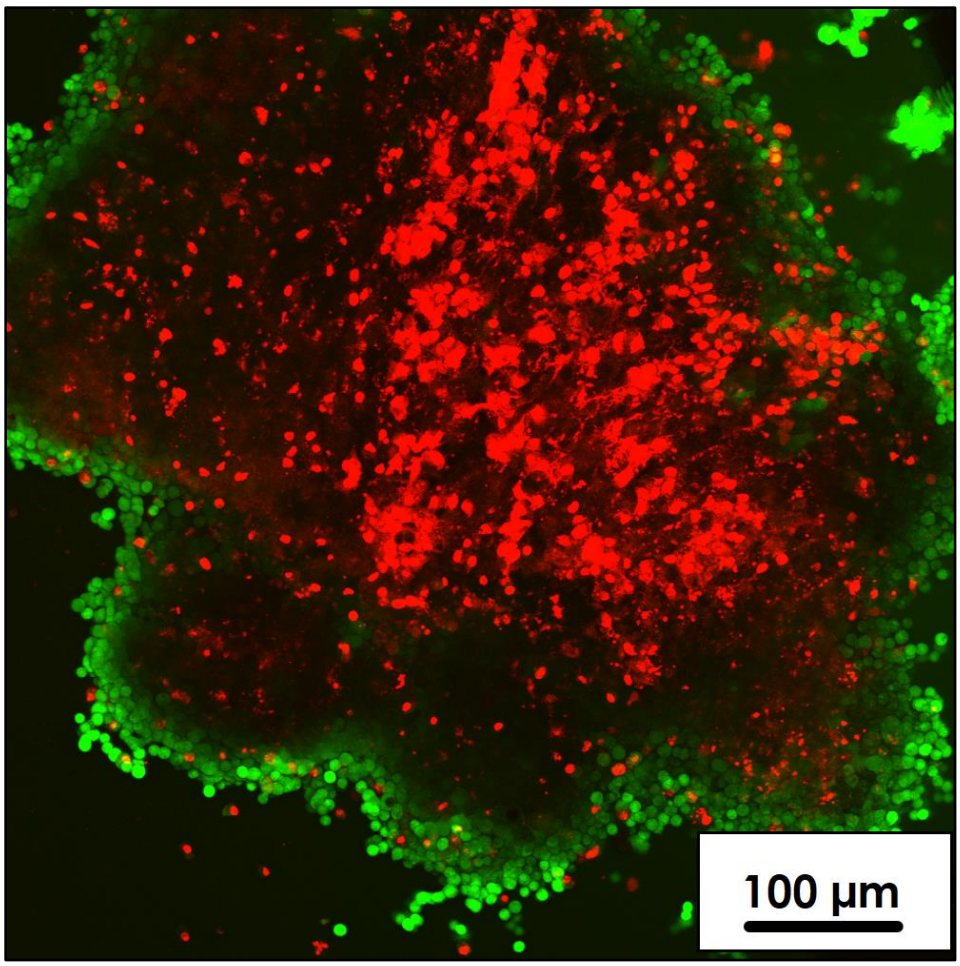

Figure 26: Fluorescent confocal microscopy of a spheroid. Green = Calcein AM, Red = Propidium Iodide. The dead core and live exterior indicates the presence of hypoxic regions observed in typical spheroids.

4.2.4. Intentional Addition of Bubbles with Cell Culture

While variation of bubble size was difficult to control due to the need to inject the bubbles past the media in the stopcock base, the variations in bubbles did not seem to produce any substantial size or morphology differences between replicates. Because of this, precisely the same means of data processing as used in section 4.2.3. was used for the data for this section. Figures 27 and 28 show representative images of spheroids gathered through the standard design bioreactors and novel bioreactors respectively when cultured with substantially sized bubbles. Note the substantial differences in size and change in total number of single cells. The novel bioreactors appear substantially closer to the images of spheroids cultured under ideal conditions as seen in section 4.2.3. Figure 29 shows the comparison of the average of medians and shows a stark difference between the novel designs and the standard designs when bubbles are added. Figure 30 shows the combined values of medians in the systems with and without bubbles. The data shown provides the clearest indication that the novel system appears capable of generating spheroids in low shear conditions despite the appearance of bubbles. Skipping showing the data isolated to this group, Figure 31 shows the average percent circularity (a function of the area over the perimeter) of the combined bubble and no bubble groups.

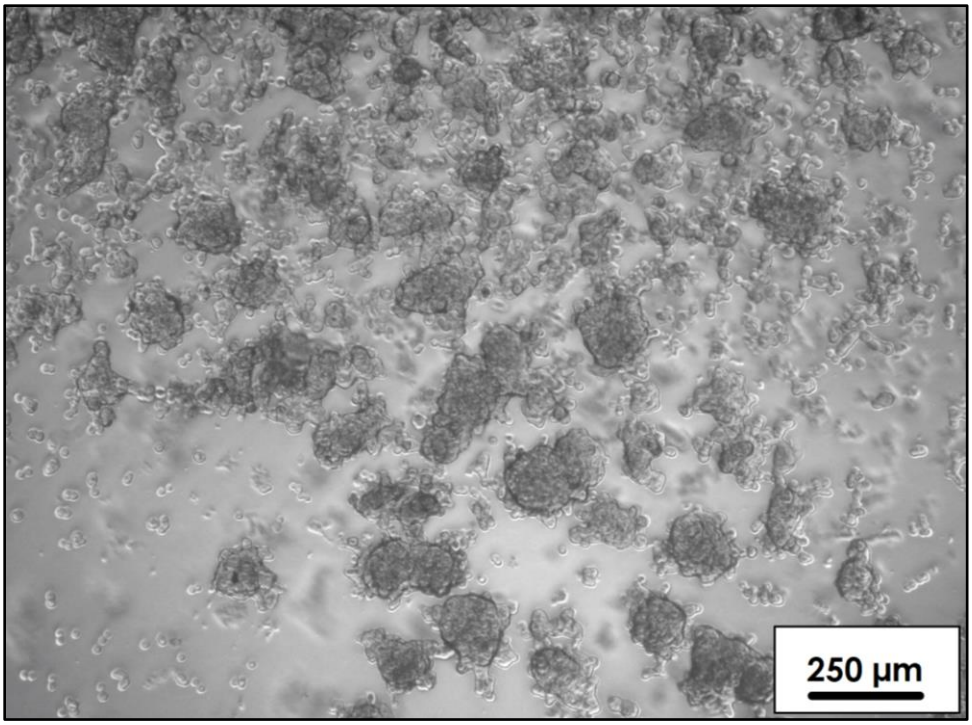

Figure 27: Spheroids formed in the standard design HARV in the presence of a bubble.

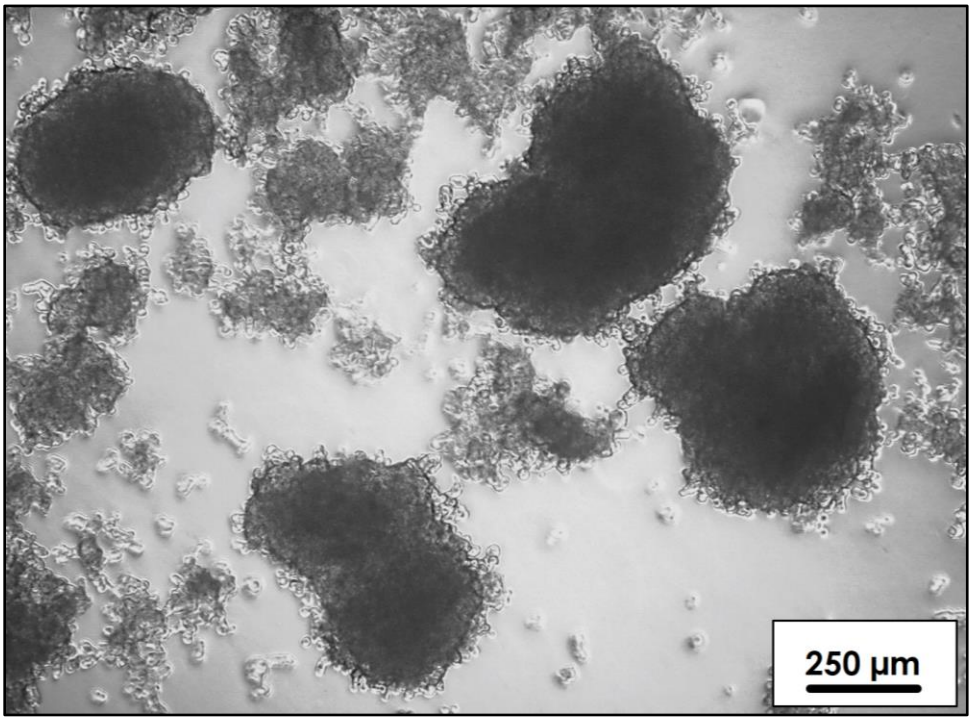

Figure 28: Spheroids formed in the novel design HARV in the presence of a bubble.

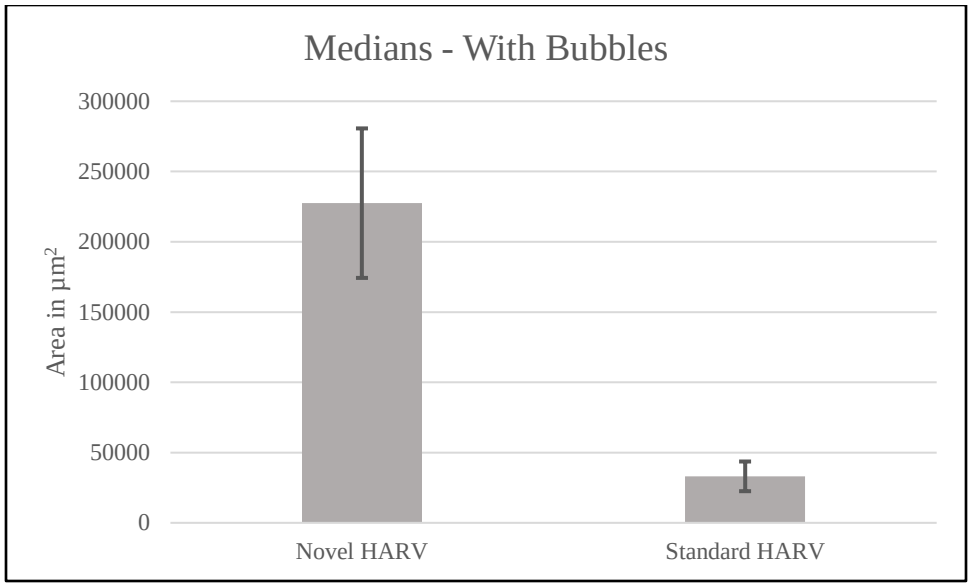

Figure 29: Average of medians of area in micrometers squared in HARVs cultured in the presence of a bubble. The difference between the two figures is extremely significant with a p-value of 0.0004.

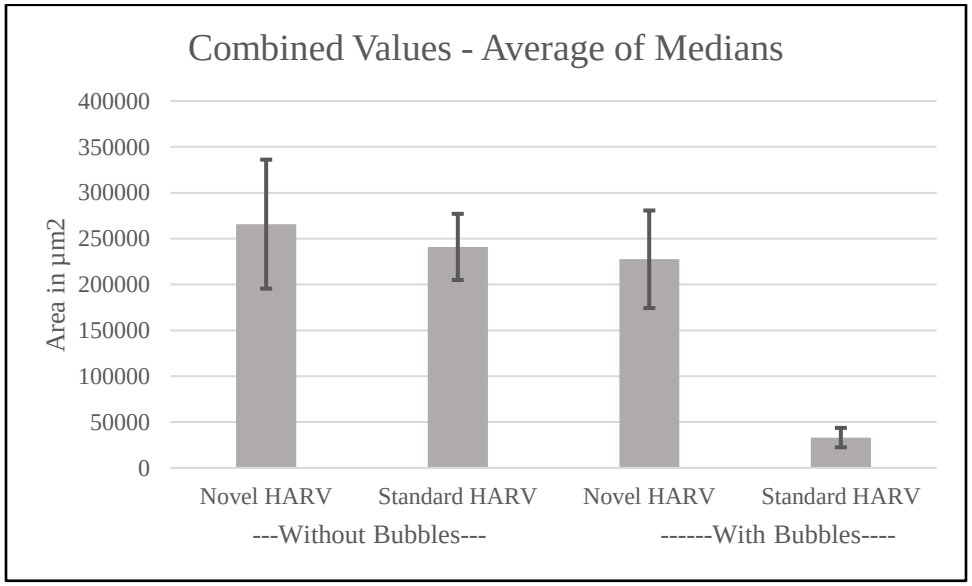

Figure 30: Combined values of figures 4.2.3.C. and 4.2.4.C., representing median area of spheroids obtained from each system. The differences between the first three figures are not significant, while there is significance between the fourth value (spheroid area from a standard HARV with a bubble) and any of the other three values. Specifically, the p-value between the novel HARVs with and without bubbles is 0.4185.

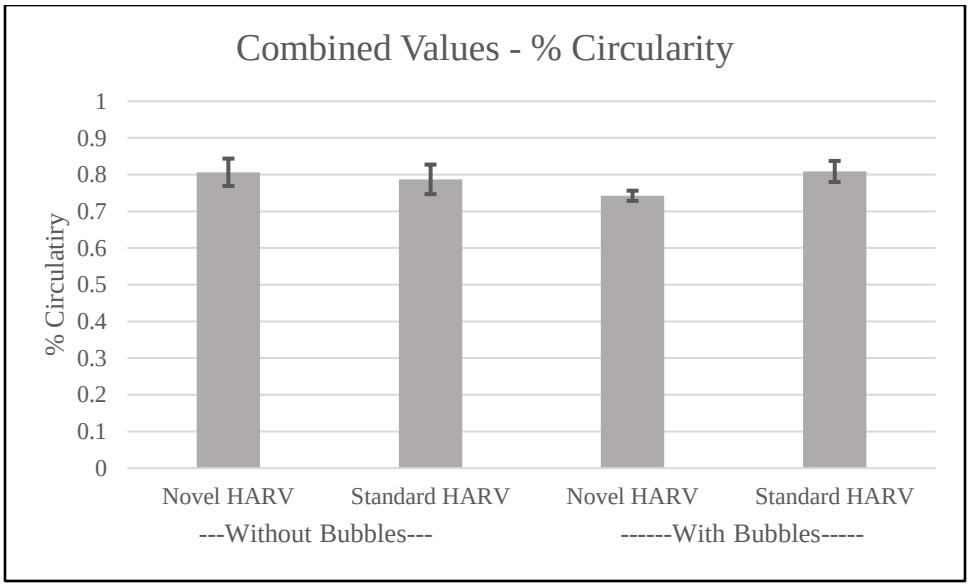

Figure 31: Combined percent circularity of spheroids cultured in novel and standard design HARVs under both without and with bubbles. There is a statistically significant difference between circularity of the novel and standard designs from the "with bubbles" group with a p-value of 0.0396.

4.2.5. Channel Capture of Cells

A total of five replicates were performed of the channel capture experiment. Values were taken and averaged, and microscopy images were taken of the relative cell densities of the main body volume and the channel volumes. Figure 32 shows one such example of the different cell densities of the two volumes. A clear difference is visible. Figure 33 shows the average ratio of the total cell count between the two volumes taken from each replicate. Cell count and ratio are described. Cell concentration is not a reliable metric to assess the probability of cells entering the channel. This is because, should this system enter an extreme failure due to channel capture, it would be expected that virtually all of the cells would migrate into the channel. With average channel capture fraction of less than 10% after 24, these results clearly demonstrate the channel capture should not be a substantial concern in cell culture using the novel designs.

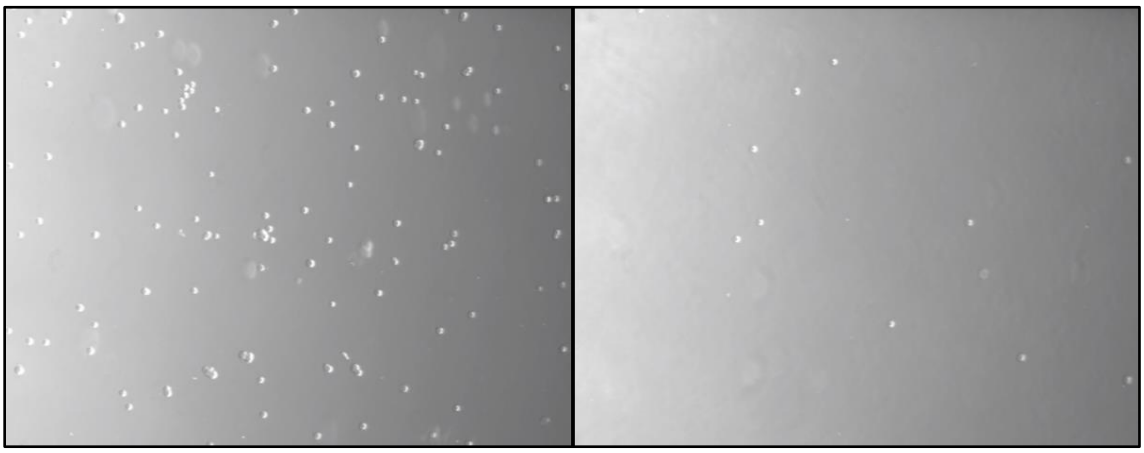

Figure 32: Observed cell counts in the novel bioreactor main volume (left) and channel volume (right).

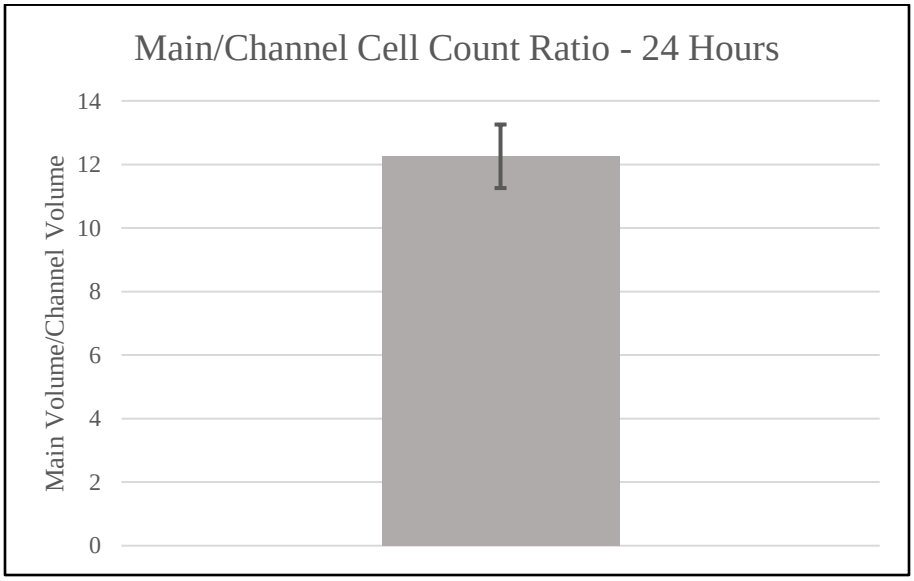

Figure 33: Ratio of total cells in main volume of the novel HARV design over the channel volume after 24 hours.

CHAPTER 5

DISCUSSION

With the RWV bioreactor's continuing and growing role in the rapidly expanding fields of both organoid and microgravity biology, improvements to existing designs may not only promote the use of the RWV but expand the success of future researchers' pursuits. The purpose of this thesis was to demonstrate the feasibility of one modification that may make the RWV a more robust and reliable cell culture system. By eliminating the detrimental effects of air bubbles to fluid dynamics, the novel HARV design may enable more consistent cell culture experiments that are less prone to failure or errant results. To evaluate the success of this objectives of this thesis, detailed analysis of the results, their limitations, and future goals that may allow for continued advancement of this technology must be discussed.

5.1 Modeling and CFD

In determining an effective modification to the RWV, the first objective was to ascertain the significance of bubbles in RWV bioreactors and to conceptualize how a bubble removal system might operate. There are two considerations that may affect the validity of a simplified bubble shear model. First of all, because any individual aggregates are freely suspended in a fluid, the experience of a strong shear force in any one direction may induce rotation rather than a surface shear effect functionally decreasing calculated shear. Secondly, because turbulence around the low pressure eddy current in the bubble containing model was not taken into account and that turbulence may induce shear an order of magnitude higher than that estimated, calculated shear may be substantially higher [67].

Subsequently, these two considerations taken together are expected to place the calculated shear values near the correct order of magnitude.

Next, because the predicted motion of a bubble in channel was clearly demonstrated to be accurate in actual operation of the finished devices, the potential flow around the entrance to the channel port is harder to demonstrate experimentally. The expectation of the behavior of the channel volume as a solid body when rotating is best validated through CFD analysis in ANSYS. The purpose of performing a simulation of fluid flow in a standard design RWV was to provide a direct comparison with the fluid dynamics in the novel design. As seen in Figures 15 and 16 while the velocity of fluids moving in a circular solid body motion did more closely resemble the behavior of a standard design as time passed, the velocity of fluids in channel stayed substantially slower than that found in the main volume. Additionally, and most importantly, the velocity of fluids in the channel did not appear to change over time as equilibrium was established in the main body. This provides a strong indication that the novel design should perform as demonstrated in the mathematical model.

One of the greatest limitations of the CFD performed was the inability to simulate the appearance of a bubble in each system. While there is no expectation of net flow in the novel design as a result of a bubble presence, the motion of a bubble in the channel during rotation as described in Figure 3 may lead to a pressure drop in the channel while the bubble is moving (according to Bernoulli's Principle of moving fluids) that normalizes when bubble motion relative to the fluid stops. This pressure change would not affect flow at the entrance in an incompressible system, but because the air bubble is compressible, the motion may lead to pulsatile fluid flow through the channel which is extended to the

channel entrance [68]. The likelihood of this appearing in a real system was evaluated in the second aim during fluid dynamic validation using alginate beads.

5.2 Design and Fabrication

While, in practice, multiple design and fabrication iterations were necessary to settle on a finalized design, there was a successful fabrication of leak-proof, non-cytotoxic, and gas permeable bioreactors. As stated previously, there is no intention for these materials and designs to be considered marketable as a full release, however, their capacity to grow healthy spheroids and culture cells for extended periods of time is a strong indication in their suitability as cell culture devices. To this end, should new experiments and designs be required, very similar materials and fabrication techniques would likely be employed.

5.3 Alginate Beads

The use of alginate beads for the validation of fluid dynamics of these systems proved to be one of the most substantial evaluations performed during this thesis. First, the determination that shear on alginate particles around a reasonably small bubble was somewhere near the force found in a moderately sized artery is the strongest indication of the importance of this thesis. Significantly, despite the previously discussed literature that mentions the importance of removing bubbles, none found provided any indication of how detrimental even a small bubble could be. Should any conclusions be drawn from this thesis regarding the use of the RWV bioreactor, by far the most significant should be that even

the smallest, barely perceptible bubble should be considered a critical failure mode and should be rectified immediately.

Next, the behavior of alginate beads in the novel bioreactor design provides a strong indication of the efficacy of the bubble catch system. Although there were occasions in which beads did migrate into the channel, their probability of doing so appeared extremely low and that was not increased when a bubble was present in the channel. Furthermore, when a significantly sized bubble (> 500 µL) was present, the bead behavior in the main fluid body was no different from that observed in the novel HARV under ideal conditions. This is the greatest visual demonstration that the novel design performs as intended.

Finally, as described above in the discussion of modeling, the motion of the bubble in the channel may induce net flow changes. There was only one point at which anything of this nature was observed during alginate bead studies. Specifically, fluid flow around the channel entrance occurred when a small amount of water was accidentally spilled on the gas permeable membrane on the back side of the novel HARV. This resulted in an apparent delamination of nylon mesh and Tegaderm. As the system rotated, the water moved to deform the shape of the Tegaderm that was now substantially less rigid. This membrane deformation appeared to allow the pressure changes in the channel due to bubble motion to cause net fluid motion at the channel entrance. While this represents one possible failure mode, two key takeaways demonstrate how the novel design is effective. First, should this design be extended to commercial production, an optimized gas permeable membrane would be used so that it would be substantially less flexible, and not prone to delamination under any condition. Secondly, because an extreme failure mode had to occur before flow around the channel entrance was visible, there is a strong indication that

pressure changes in the channel due to bubble motion are generally contained to the channel and without volume changes due to some form of deformation, will not be extended to the main volume of the system.

5.4 Cell Culture Morphology

Though modeling and the alginate beads studies performed strongly indicate the novel HARV design can accomplish its intended function, the bottom line will always be cell culture results. Figure 30 is the clearest evidence that those results are significant and beneficial. The capacity for the novel design, with and without bubbles, to produce spheroids of statistically similar morphology to those found in a standard design under ideal conditions is the clearest demonstration of the efficacy of the novel design. While this thesis was limited in its capacity to evaluate expression levels and more complex organoid systems due to time constraints, the critical fluid dynamics that make the RWV enable the formation of spheroids are precisely the mechanism by which organoids can also form and microgravity is simulated. Subsequently, it is the position of this thesis that the cell culture experiments prove the capacity of the novel design to establish and maintain the unique fluid dynamic systems of the rotating wall vessel bioreactor.

5.5 Channel Capture

Through the creation of the novel design, one of the most concerning potential failure modes was the loss of cells to the channel. The channel capture experiment performed provides a clear indication that this concern is unlikely to occur on a practical level. While there is some loss of cells into the channel, there may be a silver lining to this

occurrence that may even exceed the capacity for the novel design to remove bubbles. In a standard RWV system, should aggregates form of sufficient size or density, they would "fall out" of solid body rotation and begin interacting with the wall. This would immediately invalidate the microgravity conditions and induce high shear. In a standard RWV, when the media is collected for DNA expression analysis, any cells that were not experiencing low-shear microgravity conditions would be collected, lysed, and evaluate just like any other cells. In the novel design, any cells that no longer meet the size characteristics to stay suspended in solid body rotation would eventually move to the channel. When the main volume is collected, the channel volume is left behind and the expression analysis of the evaluated cells should be significantly more consistent, with less error and a more accurate assessment of true, ideal conditions.

5.6 Future Directions

While the work of this thesis reasonably demonstrates the ability of the novel HARV to effectively resolve one of the most frequent and substantial failure modes of the RWV, continuing research may provide more significant evidence of its value and fine-tune key functionalities to advance the novel design to the precipice of its potential. In the short term, while more replicates of the existing cell culture experiments should be performed, the addition of 1, 48, and 72-hour timepoints to the channel capture experiment to better understand the distribution of cell migration into the channel. Furthermore, expansion of spheroid morphology studies from cancer cells to other aggregating cell lines, particularly to those more prone to disruption, will provide more expansive information about the behavior of aggregates in the novel bioreactor. Finally, but repeating the bubble

injection experiment to substantially smaller bubble volumes, say the 50 µL range, it will more precisely underline the importance of having a system free from bubbles.

Outside of experimental modifications, this device might benefit greatly from design modifications. These can be simple, ranging from decreasing the size of the entrance to the channel to more extreme redesigns. Once such example would be the addition of a gate at the channel entrance. This gate could be a simple piece of acrylic containing a magnet that could conditionally be moved to allow flow between the main volume and the channel volume or to prevent it. In this way, errant bubbles could be cleared from the system upon start-up and the gate closed. Then, the system is rotated, and once the main fluid volume has been brought to equilibrium (1 hour or so), the gate could be opened to clear newly forming bubbles allow cells not experiencing microgravity to be filtered from the system. Once an ideal set of design modification has been identified, this technology could be adapted to all other forms of commercially available RWVs of all shapes and volumes.

5.7 Conclusions

Ultimately, it is the conclusion of this thesis that the novel bubble segregating design solves a critically important and chronically underestimated problem with the practical function of the RWV bioreactor. The hope of this thesis is for the barrier to entry for the RWV to be substantially reduced, expanding the volume and quality of research it produces.

REFERENCES CITED

[1] T. Yao and Y. Asayama, "Animal-cell culture media: History, characteristics, and current issues.," *Reprod. Med. Biol.*, vol. 16, no. 2, pp. 99–117, Apr. 2017.

[2] R. Edmondson, J. J. Broglie, A. F. Adcock, and L. Yang, "Three-Dimensional Cell Culture Systems and Their Applications in Drug Discovery and Cell-Based Biosensors," *Assay Drug Dev. Technol.*, vol. 12, no. 4, pp. 207–218, 2014.

[3] D. Gao and Y. Chen, "Organoid development in cancer genome discovery.," *Curr. Opin. Genet. Dev.*, vol. 30, pp. 42–8, Feb. 2015.

[4] S. A. Langhans, "Three-Dimensionalin VitroCell Culture Models in Drug Discovery and Drug Repositioning.," *Front. Pharmacol.*, vol. 9, p. 6, 2018.

[5] D. Antoni, H. Burckel, E. Josset, and G. Noel, "Three-dimensional cell culture: a breakthrough in vivo.," *Int. J. Mol. Sci.*, vol. 16, no. 3, pp. 5517–27, Mar. 2015.

[6] E. R. Shamir and A. J. Ewald, "Three-dimensional organotypic culture: experimental models of mammalian biology and disease.," *Nat. Rev. Mol. Cell Biol.*, vol. 15, no. 10, pp. 647–64, Oct. 2014.

[7] "Our 3d Cell Culture Journey." [Online]. Available: http://synthecon.com/pages/our_3d_cell_culture_journey_58.asp. [Accessed: 09-Dec-2017].

[8] U. Jammalamadaka and K. Tappa, "Recent Advances in Biomaterials for 3D Printing and Tissue Engineering," *J. Funct. Biomater.*, vol. 9, no. 1, p. 22, Mar. 2018.

[9] T. W. Gilbert, T. L. Sellaro, and S. F. Badylak, "Decellularization of tissues and organs," *Biomaterials*, vol. 27, no. 19, pp. 3675–3683, Jul. 2006.

[10] P. M. Crapo, T. W. Gilbert, and S. F. Badylak, "An overview of tissue and whole organ decellularization processes.," *Biomaterials*, vol. 32, no. 12, pp. 3233–43, Apr. 2011.

[11] A. Gilpin and Y. Yang, "Decellularization Strategies for Regenerative Medicine: From Processing Techniques to Applications.," *Biomed Res. Int.*, vol. 2017, p. 9831534, 2017.

[12] P. S. Thakuri, C. Liu, G. D. Luker, and H. Tavana, "Biomaterials-Based Approaches to Tumor Spheroid and Organoid Modeling," *Adv. Healthc. Mater.*, p. 1700980, Dec. 2017.

[13] D. Dutta, I. Heo, and H. Clevers, "Disease Modeling in Stem Cell-Derived 3D Organoid Systems.," *Trends Mol. Med.*, vol. 23, no. 5, pp. 393–410, May 2017.

[14] E.-T. Verjans, J. Doijen, W. Luyten, B. Landuyt, and L. Schoofs, “Three-dimensional cell culture models for anticancer drug screening: Worth the effort?,” *J. Cell. Physiol.*, vol. 233, no. 4, pp. 2993–3003, Apr. 2018.

[15] B.-W. Huang and J.-Q. Gao, “Application of 3D cultured multicellular spheroid tumor models in tumor-targeted drug delivery system research,” *J. Control. Release*, vol. 270, pp. 246–259, Jan. 2018.

[16] K. O. Alfarouk *et al.*, “Resistance to cancer chemotherapy: failure in drug response from ADME to P-gp,” *Cancer Cell Int.*, vol. 15, no. 1, p. 71, Dec. 2015.

[17] S. Sant and P. A. Johnston, “The production of 3D tumor spheroids for cancer drug discovery,” *Drug Discov. Today Technol.*, vol. 23, pp. 27–36, Mar. 2017.

[18] S. Riffle, R. N. Pandey, M. Albert, and R. S. Hegde, “Linking hypoxia, DNA damage and proliferation in multicellular tumor spheroids.,” *BMC Cancer*, vol. 17, no. 1, p. 338, May 2017.

[19] C. D. Yeo *et al.*, “The role of hypoxia on the acquisition of epithelial-mesenchymal transition and cancer stemness: a possible link to epigenetic regulation.,” *Korean J. Intern. Med.*, vol. 32, no. 4, pp. 589–599, Jul. 2017.

[20] H. Aboulkheyr Es, L. Montazeri, A. R. Aref, M. Vosough, and H. Baharvand, “Personalized Cancer Medicine: An Organoid Approach,” *Trends Biotechnol.*, vol. 36, no. 4, pp. 358–371, Apr. 2018.

[21] C. S. Ong *et al.*, “In vivo therapeutic applications of cell spheroids,” *Biotechnol. Adv.*, vol. 36, no. 2, pp. 494–505, Mar. 2018.

[22] B. B. Ratliff and M. S. Goligorsky, “Delivery of EPC embedded in HA-hydrogels for treatment of acute kidney injury.,” *Biomatter*, vol. 3, no. 1, 2013.

[23] J. Feng *et al.*, “An injectable non-cross-linked hyaluronic-acid gel containing therapeutic spheroids of human adipose-derived stem cells.,” *Sci. Rep.*, vol. 7, no. 1, p. 1548, May 2017.

[24] B. Ebrahimi *et al.*, “Mesenchymal stem cells improve medullary inflammation and fibrosis after revascularization of swine atherosclerotic renal artery stenosis.,” *PLoS One*, vol. 8, no. 7, p. e67474, 2013.

[25] A. X. Sun, H.-H. Ng, and E.-K. Tan, “Translational potential of human brain organoids.,” *Ann. Clin. Transl. Neurol.*, vol. 5, no. 2, pp. 226–235, Feb. 2018.

[26] T. DiStefano *et al.*, “Accelerated and Improved Differentiation of Retinal Organoids from Pluripotent Stem Cells in Rotating-Wall Vessel Bioreactors.,” *Stem cell reports*, vol. 10, no. 1, pp. 300–313, Jan. 2018.

[27] M. A. Lancaster and J. A. Knoblich, “Organogenesis in a dish: modeling

development and disease using organoid technologies.," *Science*, vol. 345, no. 6194, p. 1247125, Jul. 2014.

[28] Y.-R. Lou and A. W. Leung, "Next generation organoids for biomedical research and applications," *Biotechnol. Adv.*, vol. 36, no. 1, pp. 132–149, Jan. 2018.

[29] O. C. Baltatu *et al.*, "Human Pathophysiological Adaptations to the Space Environment," *Front. Physiol. Front. Physiol*, vol. 8, no. 8, 2017.

[30] J. P. Vandenbrink and J. Z. Kiss, "Space, the final frontier: A critical review of recent experiments performed in microgravity.," *Plant Sci.*, vol. 243, pp. 115–9, Feb. 2016.

[31] S. L. Wuest, S. Richard, S. Kopp, D. Grimm, and M. Egli, "Simulated microgravity: critical review on the use of random positioning machines for mammalian cell culture.," *Biomed Res. Int.*, vol. 2015, p. 971474, 2015.

[32] G. Clément, "International roadmap for artificial gravity research.," *NPJ microgravity*, vol. 3, p. 29, 2017.

[33] "Weightlessness and Its Effect on Astronauts." [Online]. Available: https://www.space.com/23017-weightlessness.html. [Accessed: 25-Mar-2018].

[34] C. Ulbrich *et al.*, "The impact of simulated and real microgravity on bone cells and mesenchymal stem cells.," *Biomed Res. Int.*, vol. 2014, p. 928507, 2014.

[35] R. Florencio-Silva, G. R. da S. Sasso, E. Sasso-Cerri, M. J. Simões, and P. S. Cerri, "Biology of Bone Tissue: Structure, Function, and Factors That Influence Bone Cells.," *Biomed Res. Int.*, vol. 2015, p. 421746, 2015.

[36] C. Huang and R. Ogawa, "Mechanotransduction in bone repair and regeneration."

[37] S. M. Smith, T. McCoy, D. Gazda, J. L. L. Morgan, M. Heer, and S. R. Zwart, "Space flight calcium: implications for astronaut health, spacecraft operations, and Earth.," *Nutrients*, vol. 4, no. 12, pp. 2047–68, Dec. 2012.

[38] "Space Station Astronauts Lose Bone Strength Fast." [Online]. Available: https://www.space.com/6354-space-station-astronauts-lose-bone-strength-fast.html. [Accessed: 25-Mar-2018].

[39] D. Linnarsson, "Pulmonary function and cardiopulmonary interactions at microgravity.," *Med. Sci. Sports Exerc.*, vol. 28, no. 10 Suppl, pp. S14-7, Oct. 1996.

[40] D. M. Simons, E. M. Gardner, and P. I. Lelkes, "Intact T cell receptor signaling by CD4 $^{+}$ T cells cultured in the rotating wall-vessel bioreactor," *J. Cell. Biochem.*, vol. 109, no. 6, p. n/a-n/a, Apr. 2010.

[41] Y. Wang, L. An, Y. Jiang, and H. Hang, “Effects of simulated microgravity on embryonic stem cells.,” *PLoS One*, vol. 6, no. 12, p. e29214, 2011.

[42] A. J. Steward and D. J. Kelly, “Mechanical regulation of mesenchymal stem cell differentiation.,” *J. Anat.*, vol. 227, no. 6, pp. 717–31, Dec. 2015.

[43] F. D’Angelo, R. Tiribuzi, I. Armentano, J. M. Kenny, S. Martino, and A. Orlacchio, “Mechanotransduction: tuning stem cells fate.,” *J. Funct. Biomater.*, vol. 2, no. 2, pp. 67–87, Jun. 2011.

[44] B. J. Feger *et al.*, “Microgravity induces proteomics changes involved in endoplasmic reticulum stress and mitochondrial protection,” *Sci. Rep.*, vol. 6, no. 1, p. 34091, Dec. 2016.

[45] C. Wu *et al.*, “Simulated microgravity compromises mouse oocyte maturation by disrupting meiotic spindle organization and inducing cytoplasmic blebbing.,” *PLoS One*, vol. 6, no. 7, p. e22214, 2011.

[46] Y. Wang, Y. Xie, D. Wygle, H. H. Shen, E. E. Puscheck, and D. A. Rappolee, “A major effect of simulated microgravity on several stages of preimplantation mouse development is lethality associated with elevated phosphorylated SAPK/JNK.,” *Reprod. Sci.*, vol. 16, no. 10, pp. 947–59, Oct. 2009.

[47] T. I. Fuentes *et al.*, “Simulated Microgravity Exerts an Age-Dependent Effect on the Differentiation of Cardiovascular Progenitors Isolated from the Human Heart.,” *PLoS One*, vol. 10, no. 7, p. e0132378, 2015.

[48] A. Espinosa-Jeffrey, P. M. Paez, V. T. Cheli, V. Spreuer, I. Wanner, and J. de Vellis, “Impact of simulated microgravity on oligodendrocyte development: implications for central nervous system repair.,” *PLoS One*, vol. 8, no. 12, p. e76963, 2013.

[49] A. Puca, G. Russo, and A. Giordano, “Properties of mechano-transduction via simulated microgravity and its effects on intracellular trafficking of VEGFR’s.,” *Oncotarget*, vol. 3, no. 4, pp. 426–34, Apr. 2012.

[50] Nasa, “Educational Brief NASA’s Bioreactor: Growing Cells in a Microgravity Environment.”

[51] “Autoclavable Vessel Culture Systems RCCS-4H SYNTHECON.” [Online]. Available: http://synthecon.com/pages/autoclavable_vessel_culture_systems_rccs-4h_synthecon_25.asp. [Accessed: 26-Mar-2018].

[52] “Clinostat Mechanics - Dedolph.” .

[53] G. J. Lee, “Moment of inertia of liquid in a tank,” *Int. J. Nav. Archit. Ocean Eng.*, vol. 6, no. 1, pp. 132–150, Mar. 2014.

[54] L. E. S. Ramirez, “Dynamics Of A Spherical Particle In A Model Clinostat Or Bioreactor,” 2004.

[55] T. G. Hammond and J. M. Hammond, “Optimized suspension culture: the rotating-wall vessel.”

[56] A. E. Guller, P. N. Grebenyuk, A. B. Shekhter, A. V Zvyagin, and S. M. Deyev, “Bioreactor-Based Tumor Tissue Engineering.,” *Acta Naturae*, vol. 8, no. 3, pp. 44–58, 2016.

[57] D. Grimm *et al.*, “Growing tissues in real and simulated microgravity: new methods for tissue engineering.,” *Tissue Eng. Part B. Rev.*, vol. 20, no. 6, pp. 555–66, Dec. 2014.

[58] S. R. Pollack, D. F. Meaney, E. M. Levine, M. Litt, and E. D. Johnston, “Numerical Model and Experimental Validation of Microcarrier Motion in a Rotating Bioreactor,” *TISSUE Eng.*, vol. 6, no. 5, 2000.

[59] T. Hammond, P. Allen, and H. Birdsall, “Is There a Space-Based Technology Solution to Problems with Preclinical Drug Toxicity Testing?,” *Pharm. Res.*, vol. 33, no. 7, pp. 1545–51, 2016.

[60] R. Salerno-Goncalves, A. Fasano, and M. B. Sztein, “Development of a Multicellular Three-dimensional Organotypic Model of the Human Intestinal Mucosa Grown Under Microgravity.,” *J. Vis. Exp.*, no. 113, Jul. 2016.

[61] M. C. Varley, A. E. Markaki, and R. A. Brooks, “Effect of Rotation on Scaffold Motion and Cell Growth in Rotating Bioreactors.,” *Tissue Eng. Part A*, vol. 23, no. 11–12, pp. 522–534, 2017.

[62] J. A. King and W. M. Miller, “Bioreactor Development for Stem Cell Expansion and Controlled Differentiation,” *Curr. Opin. Chem. Biol.*, vol. 11, no. 4, p. 394, Aug. 2007.

[63] A. L. Radtke and M. M. Herbst-Kralovetz, “Culturing and applications of rotating wall vessel bioreactor derived 3D epithelial cell models.,” *J. Vis. Exp.*, no. 62, Apr. 2012.

[64] G. P. Botta, P. Manley, S. Miller, and P. I. Lelkes, “Real-time assessment of three-dimensional cell aggregation in rotating wall vessel bioreactors in vitro,” *Nat. Protoc.*, vol. 1, no. 5, pp. 2116–2127, Dec. 2006.

[65] H. Kudela, “Viscous flow in pipe.”

[66] N. G. Dela Paz, P. A. D ’amore, and N. D. H. Edu, “Arterial versus venous endothelial cells.”

[67] K. N. Morshed, D. Bark Jr., M. Forleo, and L. P. Dasi, “Theory to Predict Shear

Stress on Cells in Turbulent Blood Flow," *PLoS One*, vol. 9, no. 8, p. e105357, Aug. 2014.

[68] D. T. Valassis, R. E. Dodde, B. Esphuniyani, J. B. Fowlkes, and J. L. Bull, "Microbubble transport through a bifurcating vessel network with pulsatile flow," *Biomed. Microdevices*, vol. 14, no. 1, pp. 131–143, Feb. 2012.